FEUP FACULDADE DE ENGENHARIA
UNIVERSIDADE DO PORTO

FACULDADE DE FARMÁCIA
UNIVERSIDADE DO PORTO

Mestrado em Engenharia Biomédica

Development and Characterization of Nanocarrier Systems for the Delivery of Antitubercular Drugs

Master Thesis developed in the course of Dissertation

RICARDO LEANDRO DELINDRO RIBEIRO

Supervisor
PROFESSOR MARIA DE LA SALETTE REIS

JULY 2013

Para a Sílvia.

Para o Daniel.

Acknowledgements

For different reasons, this work would not have been possible without the support of a number of high quality individuals, surrounded by which I found myself lucky to be most of the time.

I would like to start by thanking my thesis supervisor, Salette Reis, first of all for having accepted me in her group and having trusted me with this work, but also for all the scientific, material and moral support, and mainly for making sure that everyone in the group treated me well. It must have been a hard task, I am sure.

Secondly, I would like to thank Marina Pinheiro, for all the guidance and patience in this work, (even through the rough times, the bad results, and the dangerously close deadlines), and for always being present when needed. This work would not be what it is without her.

I am in debt to a few ones that helped me with some experimental techniques: Fernanda Andrade, for the help with the MTT assays; José das Neves, for the help with the HPLC measurements; and Ana Cardoso, for the help with the DSC experiment.

I would also like to thank the ones who I shared the laboratory with, and who also shared with me their knowledge, experience and overall good mood. They told me not to write their names, but I'm not going to obey: to Catarina, Catarina, Catarina, Joana, Miriam and Nini, but also to dona Manuela, Patrícia, and Sofia. A special and warm thank you note goes out to Júlia, for all these years of healthy partnership, and for always laughing, laughing out loud.

To all my colleges in the MEB programme, specially to Raquel Almeida and André Carvalho, for all those lunatic lunches and (i)rational conversations.

A deep acknowledgement goes naturally to my parents, which are, and always will be, present in everything I do.

Finally, I would like to thank those two individuals, *homo sapiens* of the highest quality, that complete my life, and to whom this work is dedicated. To Sílvia, for always being there, for always supporting my choices, for being patient with my doubts, and, above all, for not having run away. And to Daniel, for having born at exactly the right moment.

Abstract

Tuberculosis (TB) is still an ongoing public health concern in African, Asian and South American countries, where it still has a strong prevalence, resulting in a heavy economic, social and human burden. In 2011, the World Health Organization (WHO) has reported an estimated 1.4 million deaths due to TB, a disease caused by the infection of *Mycobacterium tuberculosis* (MTb). There have been determined efforts to fight this disease, and the search for new antitubercular drugs plays a crucial role. In spite of these efforts, the most recent drug in the market dates back 50 years, and so new delivery strategies that improve the efficacy of existing treatments may become important in this fight.

The goal of this work was to develop a nanocarrier system for the delivery of antitubercular drugs. The chosen nanocarriers were lipid nanoparticles, more specifically nanostructured lipid conjugates (NLCs). These particles were loaded with two anti-tubercular drugs: rifampicin (RIF) and rifabutin (RFB). Since the lung is the primary site of infection in TB, the proposed route of administration for this strategy is the pulmonary route. Once inhaled, the particles should be able to travel to the pulmonary alveoli and reach the alveolar macrophages (AMs). Produced particles thus must have an appropriate size, otherwise they will be trapped in the upper airways or leave the lung on exhaling. Also, it is known that AMs have specific receptors that bind to sugars. Surface modification by mannose coating was performed to take advantage of these receptors and improve cellular uptake by AMs.

The developed particles were characterized in terms of size, zeta and morphology. Results showed particles with size and morphology suitable to reach the pulmonary alveoli, and loading efficiency for both drugs was above 80%. The success of mannose coating was confirmed by FTIR analysis. Cytotoxicity of the formulation was evaluated by MTT assay with three different cell lines.

Although more studies are definitely needed, the results from the present work pose a strong argument for NLCs as a promising strategy for the pulmonary delivery of antitubercular drugs.

Resumo

A tuberculose (TB) apresenta-se ainda como um problema de saúde pública considerável em países Africanos, Asiáticos e Sul Americanos, onde ainda tem uma elevada prevalência, resultando num pesado fardo económico, social e humano. Em 2011, a Organização Mundial de Saúde estimou que a TB terá sido responsável, em todo o mundo, por 1.4 milhões de mortes. A TB é uma doença causada pela infeção por *Mycobacterium tuberculosis*. Inúmeros esforços têm sido concentrados no combate a esta doença, e a pesquisa por novos fármacos tem, aqui, um papel preponderante. No entanto, e apesar destes esforços, o mais recente fármaco para o combate à TB tem já 50 anos. Novas estratégias de transporte e libertação de fármacos, que melhorem a eficácia dos tratamentos já existentes, poderão tornar-se importantes nesta luta.

O objectivo deste trabalho foi desenvolver um sistema de nanopartículas para o transporte e libertação de fármacos de combate à TB. As nanopartículas escolhidas foram nanopartículas lipídicas, mais especificamente partículas lipídicas nanoestruturadas (NLC). Nestas foram introduzidos dois fármacos: rifampicina (RIF) e rifabutina (RFB). Dado que os pulmões são o principal foco de infecção por TB, a via de administração proposta é a inalatória. Uma vez inaladas, as NLC deverão depositar-se nos alvéolos pulmonares, onde se encontram os macrófagos alveolares (AMs). As partículas produzidas deverão, portanto, ter um tamanho apropriado a este objectivo. É também conhecido que os AMs têm receptores de açúcares específicos. A superfície das partículas foi então modificada para expor moléculas de manose, com o ojbectivo de aumentar a

As nanopartículas desenvolvidas foram caracterizadas em termos de tamanho, potencial zeta e morfologia. Os resultados revelaram partículas com tamanho e morfologia adequados para atingir os alvéolos pulmonares. A taxa de incorporação para ambos os fármacos foi acima de 80%. A modificação da superfície com manose foi confirmada por análise FTIR. A citotoxicidade foi avaliada por ensaios de MTT, com três linhas celulares.

Mais estudos são definitivamente necessários, mas os resultados do presente trabalho apresentam um forte argumento a favor da utilização de NLC como uma promissora estratégia para a administração pulmonar de fármacos no combate à TB.

Contents

List of figures

List of tables

Abbreviations and symbols

AM	Alveolar macrophage
CFC	Chlorofluorocarbon
CIP	Ciprofloxacin
DCP	Dicetylphosphate
DMEM	Dulbecco`s modified eagle medium
DPI	Dry powder inhaler
DPPC	Dipalmitoylphosphatidylcholine
DSC	Differential scanning calorimetry
EPC	Egg phosphatidylcholine
FTIR	Fourier transform infra-red
HIV	Human immunodeficiency virus
IC50	Half maximum inhibitory concentration
LEV	Levfloxacin
LHLN	6-lauroxyhexyl lysinate
MBSA	Maleylated bovine derum albumine
MDI	Metered-dose inhaler
MDR	Multi drug resistant
MTb	*Mycobacterium tuberculosis*
NLC	Nanostructured lipid carrier
NP	Nanoparticle
O-SAP	*O*-steroyl amylopectin
OFX	Ofloxacin
PBS	Phosphate buffer saline
PDI	Polydispersity index
PEG	Polyethylene glycol
PLGA	Poly(lactide-co-glycolide) acid
pMDI	Pressurized metered-dose inhaler
PC	Phosphatidylcholine
PS	Pulmonary surfactant
RFB	Rifabutin
RIF	Rifampicin
SEM	Scanning electron microscopy
SLN	Solid lipid nanoparticle
TB	Tuberculosis
WHO	World Health Organization
XDR	Extremely drug resistant

ζ	Zeta

1 Introduction

1.1 Motivation

Tuberculosis (TB) is still far from being a health concern of the past. Although less frequent in European countries and North America, it has a strong prevalence in Africa, Asia and South America. In 2011, the World Health Organization (WHO) reported an estimated 8.7 million new cases and 1.4 million deaths from TB, thus making it the second leading cause of death by infectious diseases in the world. To address this heavy public health burden, in 2006 the WHO lauched the Stop TB Strategy. The goals of this strategy are, for 2015, to reduce prevalence of and deaths due to TB by 50% compared with a baseline of 1990, and for 2050, to eliminate TB as a public health problem [1].

The search for new anti-TB drugs is, of course, of key importance in this fight, but notwithstanding this search, new drug delivery strategies may also play an important role. Alternative delivery systems, such as nanocarriers for anti-TB drugs, may reduce administration frequency and shorten periods of treatment, hence improving patient compliance and efficacy of treatment, and reduce drug related toxicity [2].

This constituted the major motivation factor behind this work. It's main goal was the development of a new delivery strategy for the treatment of TB, through the use of lipid nanoparticles as carriers for two rifamycins (i.e. rifampicin and rifabutin), commonly used as anti-TB drugs. The aim of this project was to produce a nanosystem for pulmonary administration, featuring both passive and active targeting strategies, in order to improve drug uptake by alveolar macrophages.

1.2 Characterization of TB

TB is a disease caused by the infection of *Mycobacterium tuberculosis* (MTb). It can affect practically all organs of the human body, but the lung (pulmonary TB) is of particular high incidence. This is to be expected, since the infection starts with the inhalation of bacilli of MTb during breathing, leading the bacteria directly to the lung. Due to their size, the bacilli are able to reach the pulmonary alveoli, where they are phagocyted by the alveolar macrophages (AMs) [3] (Figure 1).

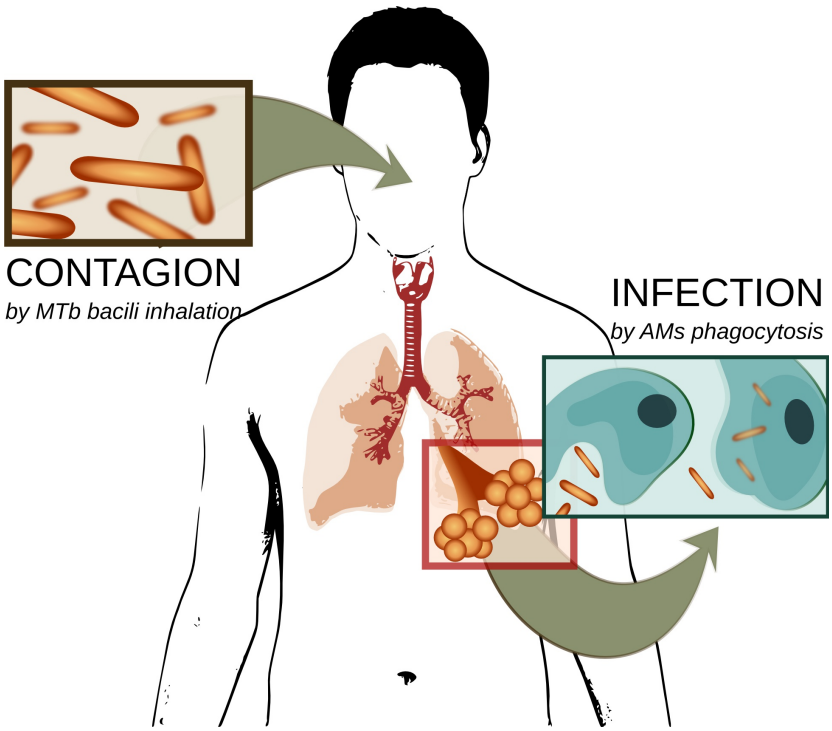

Figure 1: Contagion and infection by MTb

Inside the AMs, the bacilli reside in a membrane-bound vacuole, and for this reason some are able to avoid fusion with lysosomes and posterior digestion [4], ending up co-existing with the AMs [5]. They multiply and eventually escape the lung through the bloodstream and lymphatic system, spreading to other organs of the body, resulting in the extra-pulmonary TB [6](Figure 2). Moreover, MTb may exist within a granulomas consisting of macrophages and giant cells, T cells, B cells, and fibroblasts, and these granulomas can prevail not only in the lung, but in other organs as well. In latent infections, the state of the bacteria within the granuloma is unknown. The estimates are that one third of the world's population is infected with the organism, although usually the infection is present in its dormant state [7].

Some symptoms may be associated with pulmonary TB and extra pulmonary TB, and they could be of help when diagnosing the disease. In pulmonary TB, symptoms include cough, production of sputum in later stages (due to inflammation and tissue necrosis), hemoptysis (only in rare cases), pleuritic pain, dyspnea (unusual, unless there is extensive disease), and may also cause severe respiratory failure. X-ray of the lung and examination of sputum is often used to confirm pulmonary TB. Extra pulmonary TB has a wider range of symptoms, depending on which organ is

affected, and in many cases infection produces systemic effects, rather than local ones. Moreover, these effects are many times associated with other ailments, such as human immunodeficiency virus (HIV) infection, diabetes mellitus, and neoplastic diseases, which considerably delays diagnosis and increases misdiagnoses, specially with patients co-infected with HIV [8].

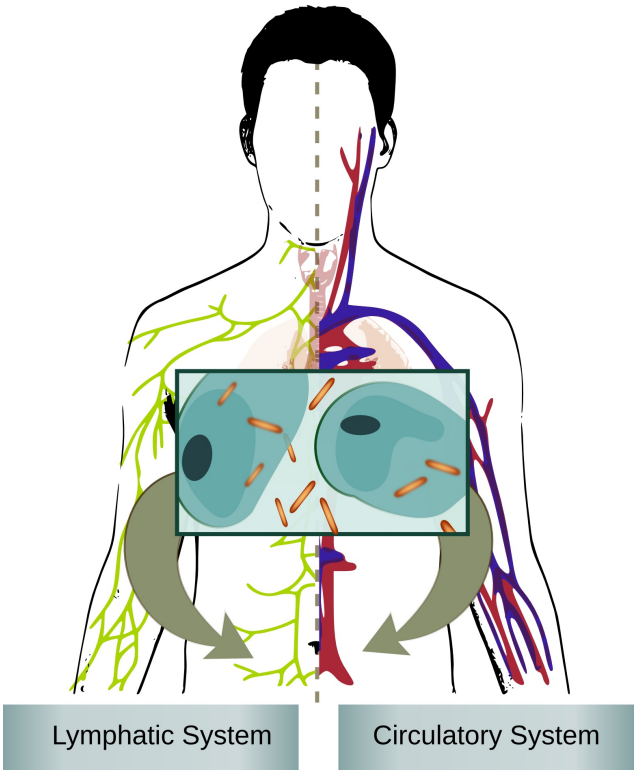

Figure 2: Extrapulmonary TB.

1.3 Traditional chemotherapy

Treatment for TB almost always involves a cocktail of drugs administrated through long periods of time, which contributes to patient non-compliance, resulting in multi drug resistant (MDR), extremely drug resistant (XDR) [1], and even totally drug resistant strains of TB, which are considerably harder to treat [9] (Figure 3). Also, progress on new drug therapies has been developing slowly, and the most recent of anti-TB drugs currently in use dates back 50 years. Sarkar *et al.*, in their review of the present TB chemotherapy available and of new and emerging drugs, stressed how essential further research in a new drug target is to fight MDR and XDR TB [2].

Currently available chemotherapy includes first-line drugs, such as isoniazid, pyrazinamide, rifampicin, and ethambutol, and second-line drugs, such as *para*-aminosalicylic acid, ciprofloxacin/ofloxacin, clofazimine, cycloserine, ethionamide, rifabutin, streptomycin, and thioacetazone [10]. These second-line drugs are only used when treatment with first-line drugs fails. They are less effective, more toxic, and unavailable in many countries due to high costs [11]. The two drugs used in the present work were rifampicin (RIF) and rifabutin (RFB). They belong to the family of rifamycin antibiotics, which are among the most potent anti-tuberculosis agents known. They possess a unique ansa structure consisting of an aromatic nucleus linked on both sides by an aliphatic bridge [12]. RIF is a red crystalline powder. It exhibits a half life between 2.3 and 5 hours on initiation of therapy, but this value decreases to between 2 and 3 hours after repeated treatment. Rifabutin (RFB) is a violet crystalline powder. It has a longest half life, between 32 and 67 hours,

but it also shows increased toxicity, and adverse effects include rash, gastrointestinal disturbance, neutropenia, and occasional uveitis [10].

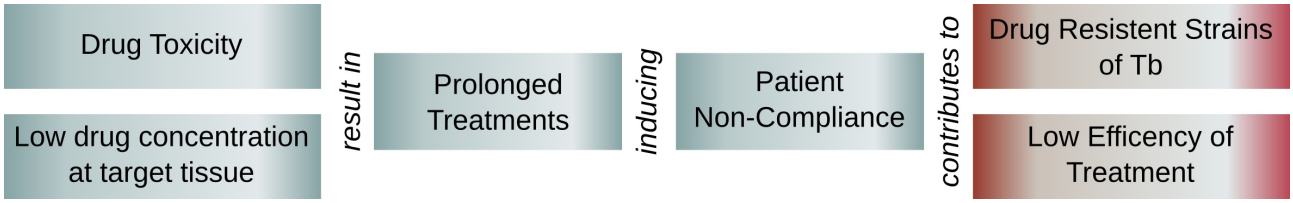

Figure 3: Problems associated with traditional TB chemotherapy.

There are several new drug candidates currently in research and in clinical trials, and several existing drugs are in a state of re-evaluation [9]. In December 2012, the FDA granted an accelerated approval of a new drug, bedaquiline, but only as part of a combination therapy to treat adults with MDR TB when other alternatives are not available [13]. However, bedaquiline has not yet gone through a phase III trial, and several accounts of heart failure have been reported, which may result in bedaquiline being removed from the market. This illustrates how important it is to find new strategies to fight this disease.

1.4 Outline of the dissertation

The present dissertation is divided in five chapters.

Chapter 1, the present chapter, constitutes a brief introduction to the theme and the main goals of the dissertation.

Chapter 2 presents some scientific considerations of TB and it's current treatment options, and it ends with a state of the art regarding nanosystems as carriers for anti-TB drugs. This state of the art, with appropriate modifications, is intended to be submitted for publication as a review article.

In Chapter 3, the materials and methods used in the present work are presented and explained.

Results from the experimental work are shown and discussed in Chapter 4.

Finally, Chapter 5 constitutes an overall reflection on the goals and achievements of this work. It also tries to outline possible paths for future work.

2 Nanosystems for the pulmonary delivery of anti-tuberculosis drugs

Since the lung is the most important point of access in the case of infection by MTb [14], [15], exploiting the inhalatory route for drug delivery becomes an exciting hypothesis to fight the disease [16]–[18]. Indeed, the lung is the ideal target site for anti-TB drug delivery, and could provide a delivery portal requiring smaller doses for efficacy, exhibiting reduced toxicity and fewer side effects [3]. Also, the respiratory system behaves as an "aerosol filter", a property that can be exploited to target particles having specific attributes to the lung [15], and since the lung mucosa has a large surface from which drugs may be systemically absorbed into the bloodstream, escaping the first-pass metabolism [14], enhancing overall bioavailability. This makes pulmonary delivery of drugs an interesting approach for the treatment of pulmonary infections. Adding to this, as was described in section 1.2, pathogenic TB bacilli establish infection mainly in alveolar macrophages [16]. In this regard, it would be of interest not only to deliver the drugs to the lung, but also to achieve phagocitosys by AMs.

2.1 Lung deposition

To achieve lung deposition, particle size is the most important characteristic to take into account [19]. Figure 4 illustrates the influence of particle size in lung deposition. Particles with diameters greater than 5 µm deposit primarily in the mouth and upper airways, while particles with diameters ranging from 1-5 µm are the most efficient to reach the deep lung. With particles bellow 1µm, mechanisms such as diffusion and sedimentation become important in reaching the pulmonary alveoli, and such could be exploited to optimize pulmonary delivery strategies [20], [21]. Particle size is also

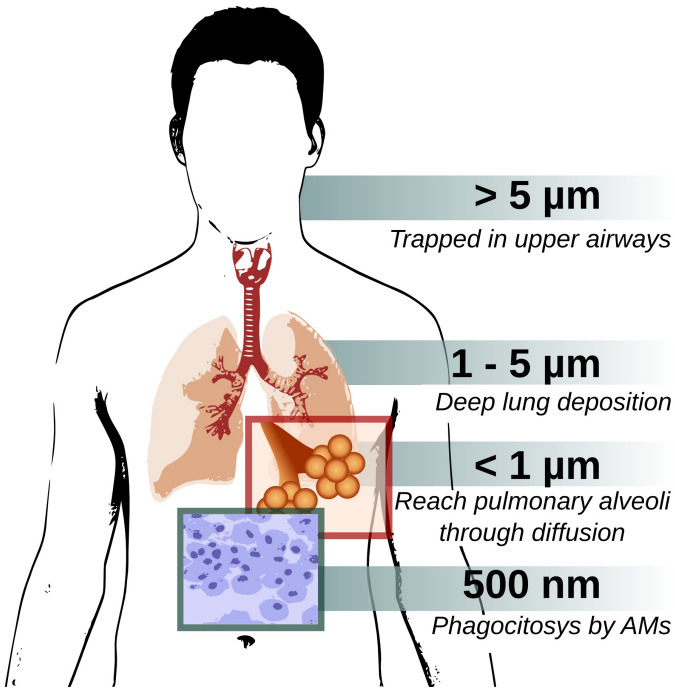

Figure 4: Influence of particle size in lung deposition and phagocitosys by AMs.

an important characteristic in passive targeting of macrophages, since they affect the success of internalization within these cells. In this regard, particles with diameters of about 500 nm have been reported as ideal to undergo phagocytosis by AMs [18].

2.2 Pulmonary administration

Pulmonary administration of drugs must be done using a suitable device. Currently, there are three main delivery devices used for this purpose: nebulisers, pressurized metered-dose inhalers (MDIs), and dry powder inhalers (DPIs). They behave differently and are used with different kinds of particles [22]. MDIs and DPIs are popular choices for the treatment of pulmonary chronic diseases. DPIs are particularly popular, since they are propellant-free, portable, easy to operate and low-cost devices. Unfortunately, dry powders tend to result in particle aggregation, increasing the aerodynamic diameter and lowering the fraction that is respirable, compromising the technique, and rendering them unable to reach the deep lung regions where alveolar macrophages lie. Nebulisers may prove to be a better choice, since they can generally produce liquid droplets which are smaller, and thereby provide the opportunity for a larger proportion of the drug to reach the deep lung regions [17].

Although promising and vastly researched, these delivery strategies face obstacles difficult to overcome. With the particular case of anti-TB drugs, so far not one formulation has reach the market [14]. These difficulties have been reported throughout the scientific literature, and include: the use of safe and accepted excipients, developing scalable processes, developing droplets with proper particle size and morphology for lung deposition, and achieving satisfactory drug loading [14]. Also, usable strategies must be able to account for different lung structures, breathing patterns, and changes in the airway morphology by the pathogenic agent [15]. They must achieve access to poorly-aerated areas of the lung and extracellular bacteria in well-aerated lung tissue, overcoming induction of resistance due to depletion of intracellular drug concentrations, and surpassing limitations due to possible innate responses of the host [23]. The use of nanosystems may be of key interest in overcoming the above-mentioned obstacles.

2.3 Active targeting of alveolar macrophages

As stated before, by fine tunning the size of the carrier system, we can enhance phagocitosys by AMs, a desirable event in the case of pulmonary TB. To this passive targeting strategy, there are active targeting strategies that can be used to improve treatment efficacy. In active targeting strategies,

the constitution and/or structure of the nanosystems is modified, so that certain ligands are present at their surface, changing the way the system interacts with surfaces and cells.

Macrophages exhibit a number of receptors that can be exploited by nanocarriers with appropriate ligands. Sugars, such as mannose [24] and lactose [25], are among the most commonly used for this purpose, since these receptors are highly expressed in macrophages. Other ligands commonly used for macrophage targeting include maleylated bovine serum albumin (MBSA), *O* - steroyl amylopectin (*O*-SAP), tetrapeptid tuftsin [26], and anionic lipids, such as dicetylphosphate (DCP).

2.4 State of the art

Nanotechnology is an area of science regarding the design and study of structures, called nanoparticles (NPs), in which at least one of the dimensions is measured at the nanoscale range (1 nm – 1000 nm). NPs display unique physical and chemical properties that significantly change with their size. In some cases, particles with dimensions greater than 1μm are considered nanoparticles, since they share some, or even most, of these physical and chemical characteristics.

NPs can be used for medical purposes, namely as nanocarriers for therapeutic and diagnostic agents by means of encapsulation, covalent attachment, or surface adsorption of these agents [27]. The use of NPs in strategies for pulmonary drug delivery is a promising area of research for several reasons. First, the size of these particles can be fine tuned to reach different areas of the lung, allowing for successful passive targeting strategies. Second, their surface can be modified and ligands attached to actively target bodies of interest, such as AMs [20]. Third, studies have demonstrated that pulmonary delivery of nanosuspensions favor higher lung tissue concentrations and markedly raise the lung to serum ratio of drugs, compared with other routes of administration [28]. This could improve bioavailability, reduce side effects, drug toxicity and dosing frequency, which ultimately leads to the increase of patient compliance and better efficacy of treatment [29].

The most frequent approach in these strategies is the use of neutral nanoparticles as carriers for the drug. Common carriers to achieve pulmonary delivery are lipid NPs, polymeric NPs and liposomes. Other formulations currently in research include the production of drug nanocrystals, aerosols with magnetic nanoparticles, nanoparticles with effervescent activity, and gold NPs for the study of internalization of NPs by AMs (Figure 5).

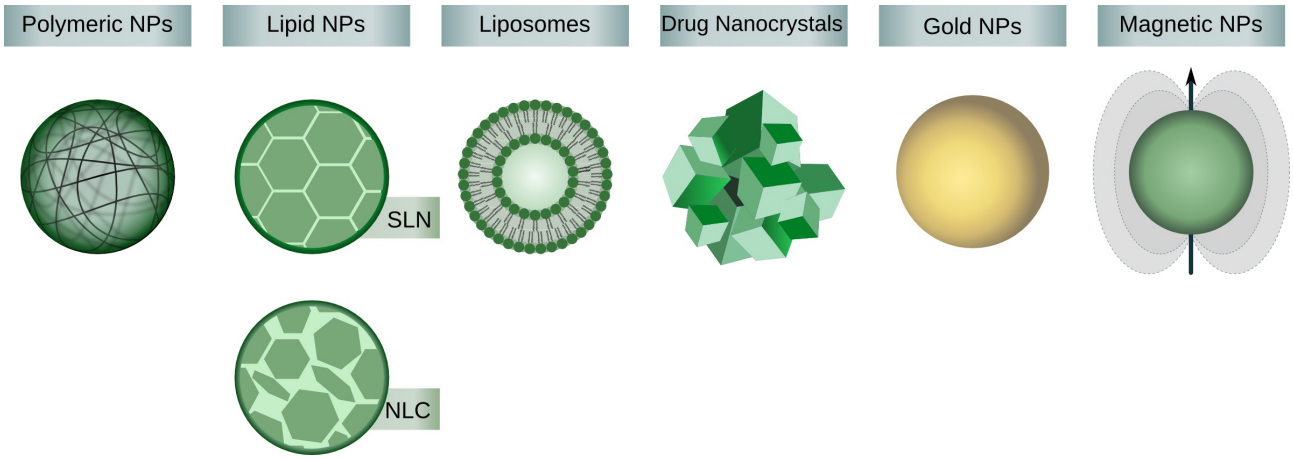

Figure 5: Nanosystems currently in study for the treatment of TB.

2.4.1 Polymeric based NPs

Natural and synthetic polymers are used to produce polymeric NPs as nanocarriers for drug delivery [30]. Polymeric NPs are among the most widely researched systems for drug delivery in general, and many reports focus on pulmonary delivery in particular. Nanocarriers consisting of poly(lactide-co-glycolide) acid (PLGA), alginate, gelatine, and chitosan are widely found in the literature. These delivery systems fulfill most requirements placed for pulmonary delivery, such as sufficient association of the therapeutic agent with the carrier particles, targeting of specific sites or cell populations in the lung, protection of the therapeutic agent against degradation, release of the therapeutic agent at a therapeutically optimal rate, ability to be transferred into an aerosol, low toxicity, and stability against forces generated during aerosolization [31]. They are also interesting materials for the engineering of biodegradable nanocarriers [32]. Many reports on pulmonary delivery using polymeric based nanocarriers have been proposed for a variety of therapeutic strategies, from gene delivery [31], [33]–[35] to more conventional drug delivery [36], [37].

Drug delivery formulations with anti-TB drugs have already been used with these nanocarriers. Jain *et al*. compared four different NP formulations for ciprofloxacin delivery, three of them being polimeric NPs [38]. The authors incorporated the drug within albumin, gelatin and chitosan NPs and studied their drug release profiles. Of the three polymers, chitosan and albumin NPs proved to be more capable of drug incorporation and sustained release.

Other studies usually focus on one type of nanosystem, although with multiple drugs. Alginate nanoparticles have been studied by Zahoor *et al*. for the incorporation of rifampicin, isonizid and

pyrazinamide [39]. The mentioned particles had aerodynamic diameters in the breatheble range, and presented high drug encapsulation efficiencies for each of the three drugs. Bioavailability of all formulations was studied, and these formulations showed better results than the administration of free drugs. Saraogi *et al*. used gelatin NPs for the delivery of isoniazid, and they associated them with active targeting by the inclusion of mannose in the formulations [40]. Their study included drug release, macrophage uptake, biodistribution and antitubercular activity studies. They obtained entrapment efficiencies of around 50%, and reported higher accumulation of isoniazid in the lungs when using mannosylated NPs, rendering them suitable for pulmonary delivery of anti-TB drugs.

Abdulla and coworkers used two different molecular weights of poly-(ethylene oxide)-block-distearoyl phosphatidyl-ethanolamine (mPEG2000–DSPE and mPEG5000–DSPE) polymers to produce nanocarriers for pulmonary delivery of rifampicin [41]. They reported high drug loading and entrapment efficiencies, and noticed that these values were influenced by drug:polymer ratio, but not by mPEG–DSPE molecular weight. Particle size and aerodynamic characterization showed that prepared formulations are suitable for lung deposition through inhalation.

Chitosan has some important reported properties to act as an inert carrier, such as biocompatibility, low toxicity and biodegradability, it is mucoadhesive and has the capacity of promoting macromolecules permeation through well-organized epithelia [42]. Moreover, it has recently been shown that cross-linked chitosan NPs can be used with pressurized metered dose inhalers (pMDIs) [43]. This recent study also showed that this approach could be used for local therapy of lung diseases, such as TB. Pourshahab *et al*. used chitosan NPs as nanocarriers for isoniazid, and obtained a release profile with an initial drug release burst, followed by slow and sustained release in the following 6 days [44].

PLGA NPs are extremely common in nanosystems, and have been used to encapsulate some anti-TB drugs. Sung *et al*. demonstrated that PLGA NPs loaded with rifampicin could be formulated, resulting in particles with aerosol properties suitable for lung delivery [45]. They have performed *in vivo* studies, and found evidence of delayed release of the drug. The presence of rifampicin in the lung was detected up to eight hours after the delivery. Jain *et al.* reported enhanced results when using PLGA NPs conjugated with lactose [25]. The conjugated particles resulted in greater average size and drug payload, slower drug release, and enhanced uptake in lung tissue, mainly due to active targeting of AMs with lactose. Pandey, Sharma and coworkers have used PLGA NPs for the incorporation of rifampicin, isoniazid and pyrazinamide, and administrated them through oral and pulmonary routes [46], [47]. They reported the presence of rifampicin in plasma

for 4-6 days, and of isoniazid and pyrazinamide for 8-9 days. Later, they reported that five doses of nebulized anti-TB PLGA NPs achieved the equivalent therapeutic benefits of 46 daily doses of orally administered free drug [46]. In 2004, the same authors, in further studies, coated similar NPs with wheat germ agglutinin, and reported an increased period during which all drugs were detectable in plasma, namely 6-7 days for rifampicin and 13-14 days for isoniazid and pyrazinamide [47].

Incorporation of hydrophilic drugs in polymeric nanosystems proves to be challenging. Cheow and Hadinoto modified PLGA preparation methods to achieve higher encapsulation efficiencies of water soluble antibiotics, using levofloxacin as the model drug [48]. They have modified the single emulsification-solvent-evaporation method by including lecithin into the aqueous phase, and the double emulsification-solvent-evaporation method by increasing the water-miscibility level of the oil phase, and succeeded in enhancing encapsulation efficiency in both cases, with no loss regarding drug release profiles and antibacterial activity after spray drying. In other instance, they developed lipid-polymer hybrid NPs to incorporate levofloxacin, ciprofloxacin, and ofloxacin [49]. After initial burst release, hybrid NPs showed a slower drug release than its non-hybrid counterparts. Table 1 summarizes the above mentioned studies on polymeric NPs.

Table 1: Polymeric NPs for incorporation of anti-TB drugs

Particle(s)	Drug(s)	Loading efficiency	Size	Ligand	*In vitro/in vivo* results	Ref.
Alginate	Rifampicin, Isonizid and Pyrazinamide	70 – 90%	~236 nm	N/A	Increase in bioavailability was confirmed. All drugs were detected: in plasma, up to 14 days; in tissues, up to 15 days.	[39]
PLGA	Rifampicin	38-42%	121-184 nm	Lactose	As compared to unconjugated NPs, lactose conjugated NPs showed greater average size and drug payload, slower drug release, and enhanced uptake in lung tissue.	[25]
PLGA PNAPs	Rifampicin	N/A	NPs: ~195 nm PNAP: ~4µm	N/A	*In vitro* release studies: 80% of drug content almost immediately released, with the remainder available for release over a period beyond eight hours . Rifampicin concentrations in the lung remained elevated for all PNAP formulations	[45]

Table 1: Polymeric NPs for incorporation of anti-TB drugs

Particle(s)	Drug(s)	Loading efficiency	Size	Ligand	*In vitro/in vivo* results	Ref.
PLGA (modified methods)	Levofloxacin	4 – 23 % (depending on the modifica-tion)	110 – 700 nm (depending on the modification)	N/A	Encapsulation efficiency was increased by employing modified methods for PLGA preparation, and drug release was maintained or improved. Antibacterial activity was maintained after spray drying.	[48]
PLGA	Rifampicin, Isoniazid and Pyrazinamide	54% for rifampicin, 64% for isoniazid and 67% for pyrazinamide	180 – 290 nm for uncoated NPs. 350 – 400 nm for coated NPs.	Wheat germ agglutinin	Presence in plasma for uncoated PLG-NPs: 4-6 days for rifampicin and 8-9 days for isoniazid and pyrazinamide. Presence in plasma for coated PLG-NPs: 6 -7 days for rifampicin and 13 -14 days for isoniazid and pyrazinamide.	[47]
PLGA	Rifampicin, Isoniazid and Pyrazinamide	57% for rifampicin, 66% for isoniazid and 68% for pyrazinamide.	186 – 290 nm	N/A	Presence in plasma: up to 6 days for rifampicin, and up to 8 days for isoniazid and pyrazinamide. All three drugs were present at therapeutic concentrations in the lungs till day 11.	[46]
MPEG2000 and mPEG5000 DSPE	Rifampicin	84 – 104%	mPEG2000: 226 – 396 nm mPEG5000: 163 – 233 nm.	N/A	*In vitro* results showed prolonged drug release over 3 days.	[41]
Chitosan	DNA plasmid encoding eight HLA-A*0201-restricted T-cell epitopes from MTb	Over 99%	~376 nm	N/A	Pulmonary delivery of chitosan-DNA nanoparticles resulted in higher IFN-γ secretion in comparison to both pulmonary DNA solution and intramuscular injection. The chitosan nanoparticles were shown to protect plasmid DNA from DNase I degradation	[50]
Chitosan	Isoniazid	17%	241 – 449nm (depending on chitosan/TTP ratio)	N/A	*In vitro* studies showed an initial burst release of isoniazid up to 4 h, followed by a more gradual and sustained release phase for the following 6 days.	[44]

Table 1: Polymeric NPs for incorporation of anti-TB drugs

Particle(s)	Drug(s)	Loading efficiency	Size	Ligand	*In vitro/in vivo* results	Ref.
Gelatin	Isoniazid	55% (uncoated) and 43% (coated)	234 nm (uncoated) and 343 nm (coated)	Mannose	*In vitro* studies show an initial burst, followed by a slower sustained release over a period of 120h. Macrophages uptake was found to be higher with coated NPs than with uncoated ones. Biodistribution studies revealed a higher drug content of INH in the liver, spleen, plasma and lung, for coated and uncoated NPs.	[40]
PC/TPGS lipid -polymer hybrid NPs	Levfloxacin (LEV) ciprofloxacin (CIP), and ofloxacin (OFX).	4-6% (CIP), 10-25%(OFX) and 10-19% (LEV)	120 – 420 nm	N/A	Drug release studies show a difference between hybrid LEV-NPs and their non-hybrid counterparts. Hybrid LEV-NPs showed a burst release in the first 5h, and then a slow release in the following 20h. With non-hybrid NPs, almost all of the drug is released in the first 5h. OFX release profiles of hybrid and non-hybrid NPs are very similar, with 90% of the drug being released in the first 5h.	[49]
Albumin, gelatin and chitosan NPs	Ciprofloxacin	48% for albumin, and 35% for chitosan. Gelatin-ciprofloxacin NPs were found to be unstable and prone to flocculation.	140 – 175 nm for albumin, 143 – 184 nm for gelatin, 247 – 322 nm for chitosan.	N/A	The aim of this study was to compare four different nanosystems: SLNs, albumin, gelatin and chitosan. *In vitro* results showed both albumin and chitosan NPs were capable of prolonged drug release up to 120h and 96h respectively.	[38]

2.4.2 Liposomes

Liposomes are vesicular structures, constituted by phospholipid bilayers enclosing an aqueous medium. They were discovered in 1965 and have been attracting interest as nanocarriers for many years [26]. They possess a unique and versatile structure, with lipid and aqueous regions, which can be altered to make them better suited to carry hydrophilic, lipophilic, or both hydrophilic and lipophilic particles. Their size can be fine tuned to achieve different regions of the lung by passive targeting, and their structure and composition can be changed to achieve active targeting to specific cells, namely AMs. Surface mannosylation is one of the most successful examples of this strategy,

as it has been shown to increase uptake of liposomes by AMs [51]–[54]. Liposomes seem particularly appropriate for pulmonary delivery, since they can be formulated from endogenous compounds, such as the components of pulmonary surfactant [55]. However, many aerosolization techniques can compromise liposome structure and integrity. In most aerosolized liposome formulations for targeted pulmonary delivery, liposomes are formed before packaging. This usually results in rupturing of vesicle structure during administration, thereby losing the ability for sustained release. However, it had already been demonstrated that PEGylated and plain Tf-conjugated liposomes are stable enough to undergo nebulisation in the course of an inhalational therapy [56]. Recently, Chattopadhyay *et al.* showed that changing their composition, by incorporation of charged lipids and cholesterol molecules into the bilayer, prevented particle aggregation and preserved bilayer integrity after air-jet nebulization [57]. Another approach is based on the fact that a drug–lipid mixture solubilized in chlorofluorocarbon (CFC) will form liposomes upon hydration in small airways. Gaur *et al*. explored the hypothesis of forming liposomes *in situ*, since the lung has a wet surface which could provide an aqueous phase for spontaneous formation [58]. They have reported that no vesicle rupture was observed with *in situ* formed liposomes, and prolonged drug release was achieved.

For all these reasons, it is therefore not uncommon to find a vast number of studies involving pulmonary delivery of drugs with liposomal formulations, many of them focusing on anti-TB drugs. Ciprofloxacin was one of the first anti-TB drugs to be used with liposomes. Wong, Finlay and coworkers explored liposomal ciprofloxacin in 1998. They studied liposome disruption during aerosolization, using 25 nebulizers [59]. Later, they published results on spontaneous formation of liposomes on dispersion of phospholipid-based powder formulations [60], [61]. With these liposomes, they achieved entrapment efficiencies of 44% for ciprofloxacin, but the value increases up to 96% with the incorporation of negatively charged lipids. Bhavane *et al*. developed liposome agglomerates that could be triggered by the instillation of a biologically acceptable agent [62]. They used cysteine as such agent, and proposed that this strategy could facilitate post-administration modulation of the drug release rate. It could allow for treatment regimens where the administration of one single dose would be sufficient for an extended period of time, since drug release could be periodically accelerated. They also found that progressive release of the drug does not cause significant inflammation, unlike the administration of free ciprofloxacin.

Other anti-TB drugs have already been studied with liposomes. Justo and Moraes studied the possibility of passive liposomal encapsulation of isoniazid, pyrazinamide, rifampicin, ethionamide,

and streptomycin [55]. However, under the tested conditions, rifampicin and ethionamide were not successfully encapsulated. Low encapsulation efficiencies were obtained for isoniazid and pyrazinamide, being the encapsulation of streptomycin only higher at a drug to lipid molar ratio of 0.04. Gaur *et al.* published a feasibility study where they used rifampicin as the model drug [58]. In this study, *in situ* formed liposomes showed better sustained release profile than the preformed liposomes, but both liposomal aerosols showed improved delivery of rifampicin over plain drug aerosols, with encapsulation efficencies around 30%. Liposomes for the delivery of isoniazid have been developed and evaluated *in vitro* [63] by Chimote and Banerjee. They observed a sustained release of isoniazid encapsulated in liposomes, tooking place over 24 h after a burst release in the first 5h. They have also conducted biocompatibility and stability studies, and found the formulations to be haemocompatible and cytocompatible, and stable for the duration of at least one month.

The possibility of surface coating to achieve active targeting with liposomes has also been a subject of interest. Vyas *et al.* used rifampicin when studying liposomes coated with macrophage-specific ligands, and reported a preferential accumulation of lingad-coated formulations in the lung macrophages, namely MBSA and *O*-SAP coated liposomes [64]. *In vivo* tissue distribution studies are on par with these results, by showing higher lung drug concentration for ligand-coated liposomes. *O*-SAP surface modification was also the focus of Deol and Khuller, who developed coated liposomes for the encapsulation of both rifampicin and isoniazid [65]. They compared the results with uncoated ones, and reported that encapsulating drugs within liposomes reduced toxicity, and that *O*-SAP coating succeeded in enhancing lung accumulation. Tuftsin functionalization of liposomes encapsulating rifampicin was studied by Agarwal and coworkers [66]. They reported interesting results: considering one single administration, tuftsin functionalization did not give better results than uncoated formulations, but with regular administration over two weeks, tuftsin liposomes were more efficient in controlling tuberculosis.

The use of aerosolized liposomes as vaccines to fight TB is a different strategy already considered. Dascher *et al.* incorporated lipids from MTb into liposomes, and administrated them to guinea pigs [67]. They succeeded in reducing bacterial burden in the lung, but regarding the spleen results were not statistically significant. Moreover, lipid-vaccinated lungs showed significantly less pathology, with granulomatous lesions being smaller and more lymphocytic.

Gene therapy has also been the subject of many studies with liposomes for the past twenty years, but despite these efforts, little progress towards developing an effective pharmaceutical product has been done, and the vast majority of clinical trials still uses viral delivery of DNA, a

much more effective approach, despite the associated toxicity issues [68]. There is ongoing research to address these problems. One recent study used single-tailed cationic lipid 6-lauroxyhexyl lysinate (LHLN) to prepare cationic liposomes, and *in vivo* results showed that, compared with commercially available Lipofectamine2000/DNA complexes, LHLN-liposomes exhibited lower cytotoxicity, and higher pulmonary gene transfection efficiency [69]. Table 2 summarizes the currently found studies with liposomes as carriers for anti-TB drugs.

Table 2: Liposomes for the encapsulation of anti-TB drugs

Particle(s)	**Drug(s)**	**Loading efficiency**	**Size**	**Ligand**	***In vitro/in vivo* results**	**Ref.**
Multilamelar liposomes (PC:Chol)	Rifampicin	47 – 49%	2 – 4 µm	Negatively charged liposomes (DCP), PE–MBSA conjugate and *O*-SAP .	Lung retention of rifampicin was higher with liposomes than with free drug. The highest value for lung retention was measured in ligand coated liposomes.	[64]
Pre formed and *in situ* formed liposomes (EPC:Chol:DCP)	Rifampicin	29 – 38%	2 and 1µm for preformed and *in situ* formed, respectivelly	N/A	There is no indication of ruptured vesicles for *in situ* formulations, and prolonged drug release is achieved. *In situ* formulations do not show any adverse effect on discharge patterns.	[58]
Liposomes (DSPC:Chol)	Isoniazid, pyrazinamide, rifampicin, ethionamide, and streptomycin.	3% for isoniazid, 2% for pyrazinamide, 0% for streptomycin and rifampicin, and 42% for ethionamide (although only at a drug to lipid molar ratio of 0.04).	286 – 329 nm	N/A	N/A	[55]
Multilamellar liposomes (DPPC)	Isoniazid	~37%	750 nm	N/A	About 50% liposome entrapped isoniazid released *in vitro* at the end of 5 h and remaining drug was released slowly over 24 h.	[63]
Liposomes (PC:Chol)	Ciprofloxacin	90% (before nebulization), of which 2 – 30% remained entrapped after nebulization, depending on the nebulizer used.	5 – 7 µm	N/A	N/A	[59]

Table 2: Liposomes for the encapsulation of anti-TB drugs

Particle(s)	**Drug(s)**	**Loading efficiency**	**Size**	**Ligand**	***In vitro/in vivo* results**	**Ref.**
Liposomes (DPPC:Chol and EPC:Chol)	Ciprofloxacin	97% before lyophilization, of which up to 90% were retained by the lyophilized cake, and up to 40% after jet milling.	1 – 7µm (lyophilized cake); 1 – 2 µm (after jet milling)	N/A	N/A	[60]
Liposomes (DPPC:CHOL: DSPE-MPEG and DPPC:CHOL:DSPE-PEG-NH_2)	Ciprofloxacin	N/A	140 – 460 nm for liposomes, depending on formulation. 1 – 140 µm for agglomerates (AVT1 and AVT2).	N/A	*In vitro* studies showed liposomes, AVT 1, and AVT 2 had an initial burst in release of drug, but it was much lower than that for free ciprofloxacin, and were capable of extended drug release in the blood. After instillation of cysteine at 90 minutes into the lungs of the rabbits treated with AVT 2, an elevation in release rate was observed.	[62]
Liposomes (DSPC:Chol)	MTb whole-lipid extract incorporated in the liposomes	N/A	< 300 nm	N/A	Lipid-immunized animals showed reduced bacterial load in the lung, but no statistically significant decreases in the spleen. Lesions in the lung tissue of lipid- and BCG-vaccinated animals were smaller, less necrotic and more lymphocytic.	[67]
Liposomes (DMPG, EPC:DMPG, and DMPC:DMPG)	Ciprofloxacin	Above 90% and around 50%, before and after nebulization, respectively.	2 – 3 µm	N/A	N/A	[61]

Table 2: Liposomes for the encapsulation of anti-TB drugs

Particle(s)	**Drug(s)**	**Loading efficiency**	**Size**	**Ligand**	***In vitro/in vivo* results**	**Ref.**
Liposomes (EPC:Chol)	Isoniazid, rifampicin	8 – 10% for isoniazid. 44 – 49% for rifampicin.	≥200 nm for *O*-SAP coated liposomes. <200nm for DSPE-PEG liposomes.	*O*-SAP	Encapuslated drugs were found to be less toxic than free drug. Drug uptake in macrophages was found to be similar between encapsulated and free drugs. Slow and controlled drug release was achieved in encapsulated drugs. *O*-SAP coating enhanced lung accumulation. Also, pre-administration of PC and Chol liposomes before the injection of lung specific stealth liposomes, further enhanced their uptake in lungs.	[65]
Liposomes (EPC)	Rifampicin.	28 – 32%	25 – 65nm	Tuftsin	With 10 mg/kg dose of liposomal RIF, a significant reduction in the lung bacillus load and an increase in MST were observed, compared with those in free RIF treated animals. Regarding tuftsin functionalization, one single treatment with coated liposomes was only marginally better than that observed with uncoated ones, but coated liposomes given twice weekly for 2 weeks was considerably more effective than uncoated ones in controlling TB.	[66]

2.4.3 Drug nanocrystals

The pure use of therapeutic agents in the form of nanocrystals has been proposed as a system for drug delivery. They are used as dispersions of pure drug nanoparticles kept stable through the presence of a minimum amount of a surfactant – nanosuspensions. Drug nanocrystals dissolve rapidly in the lung lining fluid leading to a high concentration, which is helpful for localized treatment of respiratory diseases such as pulmonary TB. Results show that these could be used in drug delivery formulations to improve pharmacokinetic, pharmacodynamic and targeting properties of poorly soluble drugs. Gao *et al.* reported two different kinds of pulmonary formulations containing drug nanocrystals [28]: aqueous nanosuspension packaged and administered by a nebulizer; drug nanocrystals collected and transported into the lung by the small aerosol droplets generated by the nebulizer.

Spore like drug particles for deep lung deposition have also been proposed as an innovative system [70]. Hollow and spore like nanoagglomerates were obtained by mixing the drug solution with an antisolvent in a high gravity environment. The fabrication of drug particles similar to spores may improve the pulmonary drug delivery efficiency in DPIs, and is a more efficient, cost-effective and easy to scale up method over milling, homogenization, spray freezing into liquid, and supercritical antisolvent precipitation to prepare nanosuspensions. According to the authors, uniform particle size and controlled morphology can be achieved with this technique.

Currently, only one report was found regarding the production of nanocrystals or nanoagglomerates of an anti-TB drug. El-Gendy *et al*. prepared ciprofloxacin nanosuspensions that were then flocculated to form nanoparticle agglomerates [71]. Nanoparticle size ranged from 68 – 722 nm, depending on the formulation, and agglomerates exhibited a particle size range of 2 – 4 μm. They performed dissolution studies, and compared the results with the stock drug. Results showed that the dissolution rate was improved, demonstrating that these techniques may help to overcome some of the solubility issues presented by new anti-TB drugs, specially by molecules that, although did not pass from the clinical trials due to solubility issues, shown higher potential as anti-TB drugs.

2.4.4 NPs with effervescent activity

Nanoparticles with effervescent activity have recently been suggested for pulmonary delivery. Oral drug delivery associated with effervescent pharmaceutical formulations is used for a long time, in stomach distress medications, vitamin supplements and analgesics. Effervescent activity of the carrier particles occurs when the carrier particles are exposed to humidity, adding an active release mechanism to the pulmonary route of administration. Additionally, effervescent particles can be synthesized with adequate size for deep lung deposition, and the technology appears to be safe for pulmonary delivery [72].

Although effervescent NPs have been mostly studied as a promising pulmonary delivery strategy for anti-cancer drugs [72]–[74], one report has been found regarding their use for the delivery of ciprofloxacin [75]. Ely and coworkers have developed and studied different powder compositions with effervescent activity, and found two formulations suitable for pulmonary delivery. These formulations had the addition of l-leucine and PEG 6000, which improved the aerodynamic characteristics of the powder particles. Effervescent activity of the prepared formulations resulted in the release of nanoparticles with less agglomeration compared to the carrier particles made just of lactose.

Table 3: Other nanosystems for the delivery of anti-TB drugs

Particle(s)	**Drug(s)**	**Loading efficiency**	**Size**	**Ligand**	***In vitro/in vivo* results**	**Ref.**
Drug nano-particle agglom-erates	Ciprofloxacin	81 – 96%	68 – 722 nm for NPs; 2 – 4 μm for NP agglomerates	N/A	N/A	[71]
PBCA Effervescent NPs	Ciprofloxacin	N/A	Carrier particles: 2μm Effervescent preparations: 244 and 252 nm before and after spray drying, respectively. Effervescent preparations containing l-leucine and PEG 6000: 150 and 177 nm, before and after spray drying, respectively.	N/A	Effervescent carrier particles released 56% ciprofloxacin into solution compared with 32% when lactose particles were used.	[75]

2.4.5 Gold and magnetic NPs

Gold NPs have recently been used to study internalization and intracellular translocation of inhaled nanoparticles in rat AMs [76]. Particles used had mean hydrodynamic radius of 16 nm. Results showed AMs had efficiently internalized NPs by endocytosis. Gold NPs have been conjugated with streptomycin [77], and it has been demonstrated that ciprofloxacin binds to gold NPs [78], but the cited studies do not focus on pulmonary delivery, and no other reports have been found regarding the use of these particles for pulmonary delivery, regardless of the model drug.

The use of magnetic aerosols using superparamagnetic iron oxide NPs has also been suggested as a way to improve drug delivery to the lung [79], and ciprofloxacin has been used as a model drug in the development of superparamagnetic nanocomposites with magnetically mediated release of the loaded anti-TB drug [80]. However, no study has been found combining these two strategies to achieve magnetically mediated pulmonary delivery of anti-TB drugs.

2.4.6 Lipid NPs

Lipid NPs are the last nanosystems presentd in this state of the art and are the focus of this thesis. Generally speaking, and by contrast with liposomes and polymeric nanoparticles, lipid NPs show higher drug loading capacity, higher stability, and require the use of lower amounts of organic solvents during production [81]. As with liposomes and most polymeric NPs, these nanocarriers are biocompatible and can be produced with appropriate size and morphology for lung targeting and deposition [82], and have been studied as a viable pulmonary drug delivery strategy [83]. It is also possible to modify the surface of lipid NPs to achieve active targeting of AMs. Mannose is a common surface modification with lipid nanocarriers [84].

Solid lipid nanocarriers (SLNs) and nanostructured lipid carriers (NLCs) are the two most common lipid NPs used. The published results by Jain and coworkers, who compared four different nanocarriers for the incorporation of ciprofloxacin, showed that SLNs are capable of prolonged drug release [38]. This work is one of the three reports that were found regarding pulmonary delivery of SLNs loaded with drugs for the treatment of TB, namely rifabutin, isoniazid, rifampicin and pyrazinamide. Nimje *et al*. prepared rifabutin loaded SLNs, and compared uncoated formulations with formulations coated with mannose [24]. Results showed cellular uptake in AMs was almost six times enhanced due to mannose coating. Coated formulations also showed to be less immunogenic and more suitable for sustained delivery. Pandey and Kuller have prepared SLNs for pulmonary delivery through nebulization [85]. They incorporated isoniazid, rifampicin and pyrazinamid, of which rifampicin showed the highest incorporation due to the lipid-based nature of the formulation and lipophilic characteristics of the drug. The nebulized SLNs were successfully deposited in the lungs, and were detected in other organs up to 7 days after administration. Administrated free drug was cleared from the system within 24 – 48 h. Jain and Banerjee included SLNs in their list of nanosystems to deliver ciprofloxacin, and concluded that these NPs were suitable for drug loading, and capable of sustained drug release [38].

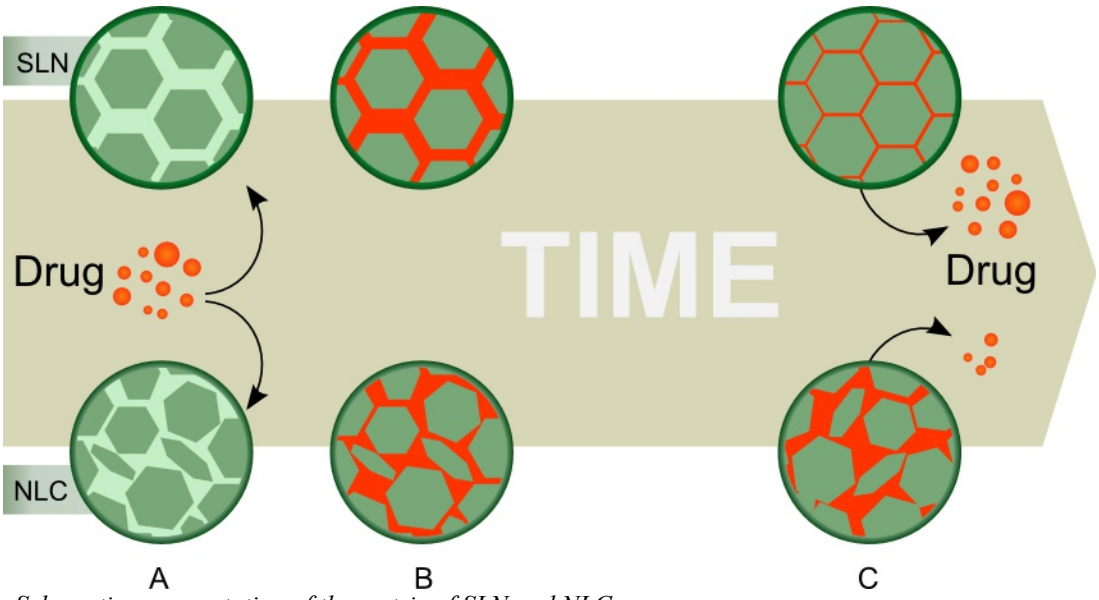

Figure 6: Schematic representation of the matrix of SLN and NLC.

A:SLN exhibits a high order matrix, while NLC exhibits a low order matrix. B: Drug is loaded into SLNs and NLCs. C: Over time, SLNs tend to a denser lipid packaging and higher drug expulsion than NLCs.

The matrix of SLNs consists of solid lipids only, with perfect crystallinity. This results in lower drug loading, since there are very few empty spaces in which the drug can be found. It also results in expulsion of drug content during long storage due to changes in lipid packaging. NLCs are different structures. The matrix consists of both solid and liquid lipids, consequently showing lower crystallinity and higher incidence of nanostructures, which won't result in denser lipid packaging over time. Thus, higher drug loading and stability during long storage is achieved, when compared with SLNs [86]. Figure 6 illustrates the differences in the matrix of SLNs and NLCs, and the overall influence of such differences in drug loading and expulsion over time. However, it should be noted that no study was found regarding the use of NLCs as carriers for any anti-TB drug. Table 4 summarizes currently found studies regarding the use of lipid nanoparticles for the treatment of TB.

Table 4: Lipid NPs for the incorporation of anti-TB drugs

Particle(s)	**Drug(s)**	**Loading efficiency**	**Size**	**Ligand**	***In vitro/in vivo* results**	**Ref.**
SLN (tristearin)	Rifabutin	82% (uncoated) and 87% (coated)	251 nm (uncoated) and 389 nm (coated)	Mannose	*In vitro* studies showed a sustained drug release for 120h, during which uncoated SLNs showed higher drug release. Macrophage uptake was higher for coated SLNs. *In vivo* results showed higher drug presence for coated SLNs in the lungs.	[24]
SLN (Stearic acid)	Isoniazid, rifampicin and pyrazinamid	51% for rifampicin, 45% for isoniazid and 41% for pyrazinamide.	1 – 2 µm	N/A	*In vitro* results varied for simulated gastric or intestinal fluid. The drug released was <20% in the first 6 h and 11–15% during 6–72 h for isoniazid/pyrazinamid; 9% in the first 6 h and 11% during 6–72 h for rifampicin, although rifampicin release was in the range of 8–12% during the entire study period for intestinal fluid. All the three drugs could be detected in the lungs, liver and spleen of the animals up to day 7 following the nebulization.	[85]
SLN (stearic acid)	Ciprofloxacin	39%	74 – 99 nm	N/A	The aim of this study was to compare four different nanosystems: SLNs, albumin, gelatin and chitosan. *In vitro* results showed SLNs were capable of a prolonged drug release up to 80 h.	[38]

3 Materials and Methods

3.1 Development of Nanostructured Lipid Carriers

3.1.1 Initial formulation

NLCs were initially prepared with with Cetyl Palmitate ($C_{32}H_{64}O_2$; M=480.83 g $mole^{-1}$; Gattefossé) as the solid lipid, and Mygliol 812 (from Acofarma) as the liquid lipid. Polysorbate 60 ($C_{64}H_{126}O_{26}$; M=1 310 g mol^{-1}; Sigma Aldrich) was used as surfactant, to stabilize the emulsion. Quantities used for each are presented in table 5:

	Mass / mg
Cetyl palmitate	350
Mygliol 812	150
Polysorbate 60	100

Formulations prepared with 4.4 g of ultrapure water.

There are several methods to produce NLCs in the laboratory, such as high pressure homogenization, microemulsion technique, emulsification-solvent evaporation, emulsification-solvent diffusion method, solvent injection (or solvent displacement) method, phase inversion, multiple emulsion technique, ultra-sonication and membrane contractor technique [86].

In the present work, an ultra-sonication method was used. In detail, the two lipids and the surfactant were heated in a water bath up to 70º C, temperature at which both lipids are in the liquid state. When the solid lipid was fully melted, 4.4 mL of heated ultrapure water (T = 70º C) was added to the mixture. Mixture then went through ultraturrax (Ystral X10/20 E3) at 3500 rpm for 30 s, and sonication (Sonics Vibra-cell, with CV18 probe) at 70% power for 5 min, which resulted in a nanoemulsion. This nanoemulsion was finally left to cool at room temperature and stored. Figure 7 features a schematic representation of the process.

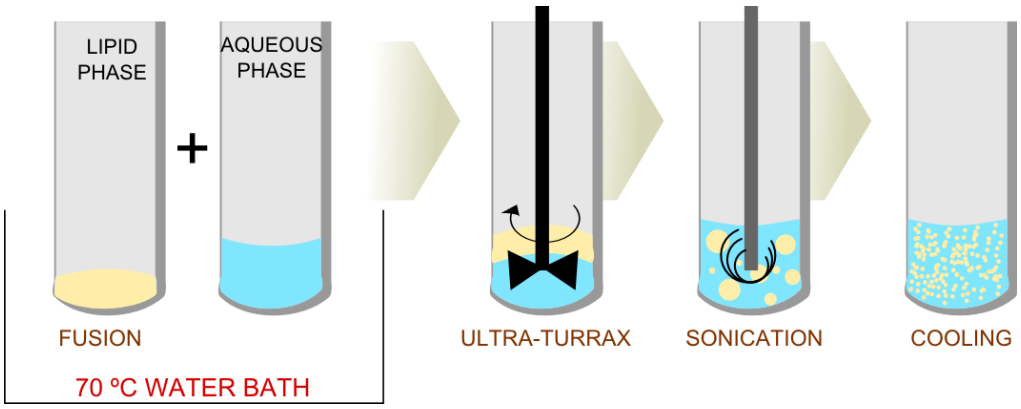

Figure 7: A schematic representation of the steps performed to develop simple NLCs.

3.1.2 Drug Loading

Two anti-TB drugs were used in the present work, one first-line drug (RIF) and one second-line drug (RFB). A third first-line drug (isoniazid) was considered, but its high hidrofilicity rendered it unsuitable for lipid NPs. RIF ($C_{43}H_{58}N_4O_{12}$; M=822.94 g mol^{-1}; Sigma Aldrich) and RFB ($C_{46}H_{62}N_4O_{11}$; M=847.00468 g mol^{-1}; Sigma Aldrich) are lipofilic molecules, and in principle suitable to be loaded with high efficiency in lipid NPs.

Drug content in loaded NLCs (NLC-RIF and NLC-RFB) was added (~7 mg) to the lipid mixture prior to the melting stage. When the melted lipid mixture and the drug form a homogeneous liquid mixture, ultra-pure water is added, followed by ultraturrax and sonication, as described before.

3.1.3 Choice of solid lipid for improved drug loading

Drug loading and release are essential parameters to evaluate a drug delivery system. Solubility of the drugs in the lipid mixture plays a major role in the amount of drug a nanosystem can be loaded with. When it comes to lipid NPs, it is important to choose lipids where the used drugs exhibit high solubility. For this purpose, qualitative solubility studies where performed to choose a solid lipid that would yield better results than the initially used Cetyl Palmitate.

In brief, the same amount of rifampicin was added to the same amount of five solid lipids: Cetyl Palmitate, Dynassan 116, Compritol 888 ATO, Golucire 43/01, Precirol ATO 5 (all lipids from Gattefossé). Lipids Compritol 888 ATO and Precirol ATO 5 both gave satisfactory results, showing the highest solubility for the used drugs. However, Compritol 888 ATO has a much higher melting

point (above 70 ºC) and it was deferred in favor of Precirol ATO 5. The final lipid mixture used in the formulation was Precirol ATO 5 as the solid lipid, and Mygliol 812 as the liquid lipid.

3.1.4 Mannose coating

As described in detail in the state of the art, mannose ($C_6H_{12}O_6$; M=180.16 g mol^{-1}) has already been used to enhance uptake by AMs with gelatin NPs [40], liposomes [51] and SLNs [24], and it was chosen as the ligand in the presented work to achieve active targeting.

Coating of NLCs with mannose (NLC-M) was initially adapted from the methods described by Jain *et al.* for SLNs used for site specific delivery of anti-cancer drugs [87]. First, NLCs were modified in order to exhibit amine groups at the surface. To achieve this, stearyl amine (Octadecylamine; $C_{18}H_{39}N$; M=269.51 g mol^{-1}; Sigma Aldrich) was added to the lipid mixture described at 3.1.3, and the resulting mixture was dissolved in acetone:ethanol (1:1 v/v) at 70ºC. An aqueous phase was prepared, containing the surfactant and the drug. The lipid phase was slowly mixed with the aqueous phase, at 70ºC, using a micropipette, while slowly agitating. The mixture was then ultraturraxed and sonicated as described before. For mannosylation of NLCs, a mannose (Sigma Aldrich) solution (50 mM) was prepared in acetate buffer (pH = 4), and subsequently added to the NLC suspension and left under constant and gentle stirring for a period of 48h. The rationale behind this procedure follows: the acidic environment would result in the ring opening of the mannose molecules; the aldehyde group would then react with free amine present at the surface of the stearyl amine functionalized NLCs, leading to the formation of a Schiff's base (–N=CH–) (Figure 8), which can be detected using Infrared Spectroscopy.

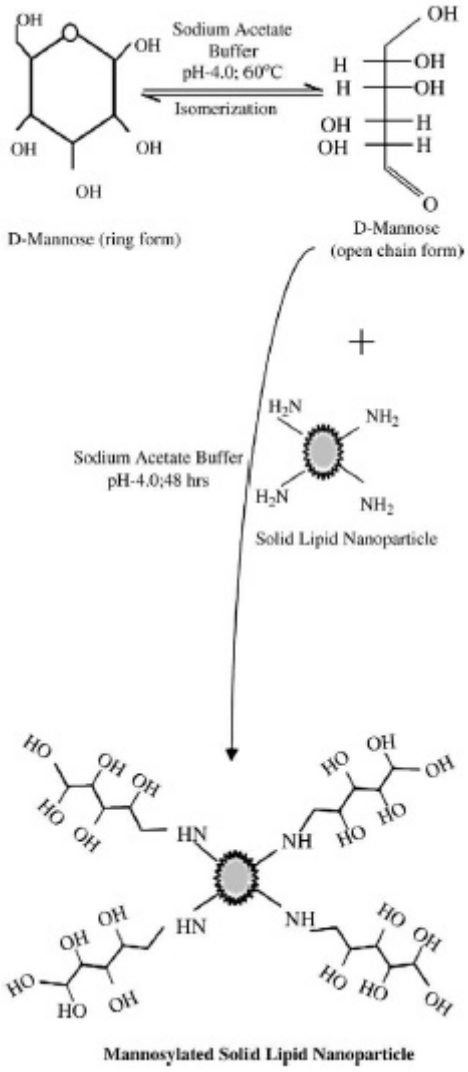

Figure 8: Schematic representation of method for mannosylation of SLNs.[87]

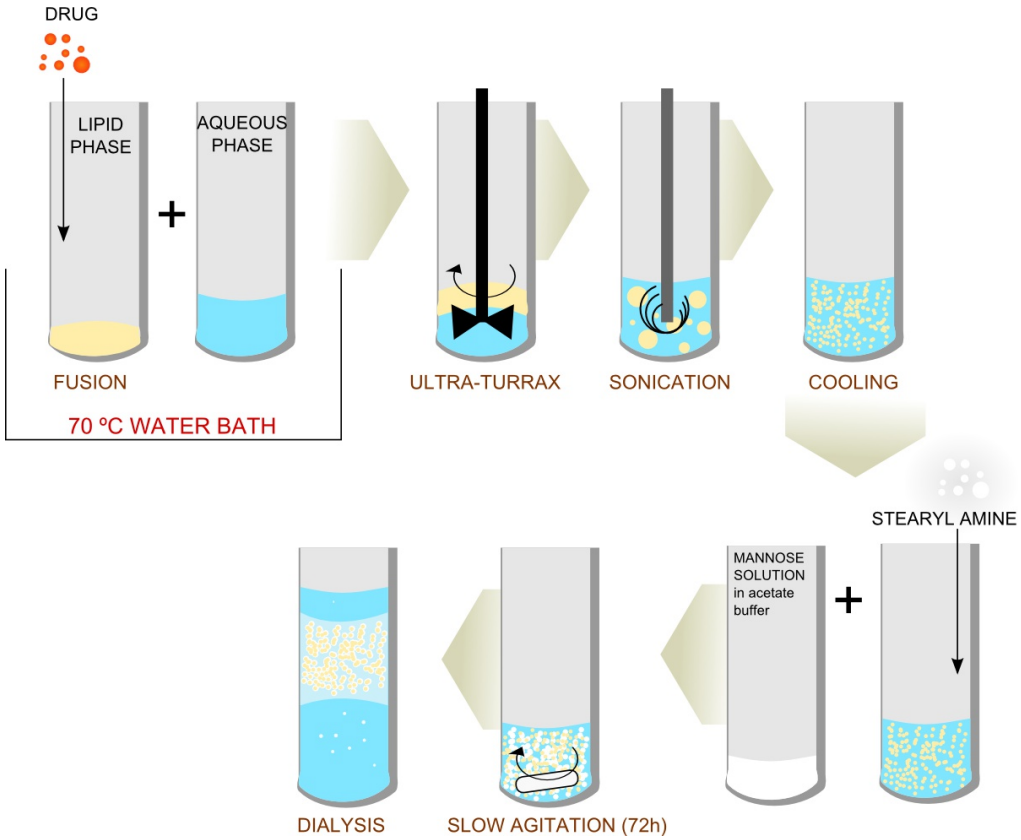

Figure 9: A schematic representation of the final process to achieve mannose coated, drug loaded NLC suspension.

This first method resulted in a very thick formulation, and modifications were performed to achieve a workable liquid suspension, as well as to try to avoid using an organic solvent in the process (acetone). The final method consisted in the development of the NLCs as described in 3.1.1, with the lipid mixture stated in 3.1.3, to which the drug content was added. Afterwards, the solution of mannose in acetate buffer was added to the NLC suspension, together with stearyl amine. The mixture was then left under constant and gentle stirring for a period of 48h. Finally, the resulting suspension was washed through dialysis in ultra-pure water for 30 min, using a regenerated cellulose tubular membrane (CelluSep T3; Nominal MWCO: 12 000 – 14 000; Wall thickness: 20 µm; Orange Scientific), to remove any excess mannose and stearyl amine. Figure 9 shows a schematic representation of the final process to achieve mannose coated, drug loaded NLCs.

3.1.5 Lyophilization

Lyophilization (or freeze-drying) is the process of removing water from a frozen sample, using sublimation and desorption under vacuum. Many pharmaceutical products, mainly heat sensitive com-

pounds, are dried using this technique, since it improves the long-term physico-chemical stability and prevents degradation reactions such as hydrolysis. Lyophilization is also used with NPs to prevent particle aggregation [88].

Liofilization was the final step of the present formulation, not only to improve physico-chemical stability, prevent degradation and particle aggregation, but also to allow a successful detection the Schiff's Base (thus confirming mannose coating) using Infrared Spectroscopy, and to provide a better material to perform citotoxicity studies, since re-suspension could be done using cell medium. The quality of the lyophilized product is highly dependent on the parameters of the process. The ideal lyophilization parameters for NLCs were based on the literature. Varshosaz *et al.* performed an exhaustive study on lyophilization parameters of NLCs, experimenting with various temperatures, pressures and cryoprotectants [88]. Considering the differences in materials available, a lyophilization process for NLCs was adapted from the procedure considered ideal by Varshosaz and coworkers.

A VirTis freeze dryer (Advantage Plus EL-85; SP Scientific) was used in this process. Samples were prepared with Aerosil 2% (m/m) as cryoprotectant. Initial freezing was done at – 60 ºC for 720 min. Condensatin was made at – 80 ºC under 150 mTorr of pressure. Drying was done at 20º C for 1 200 min, under 150 mTorr of pressure. Secondary drying was performed at 25 ºC, for 1 200 min, under 100 mTorr of pressure.

3.2 Characterization

3.2.1 Particle Sizing

To determine the size of the developed NLCs, dynamic light scattering (DLS) – also called photon correlation spectroscopy – was used. The advantages of using this technique over other techniques to determine the average size of a large population of spherical particles include the short time required to perform the measurements, the statistical validity of the results and the relatively low cost of the necessary devices. There are, however, drawbacks, such as the influence in the results of dust particles and nanoparticle aggregation [89].

The determination of particle size by DLS works by studying the scattering of light by particles in suspension, assuming they are spherical in geometry and animated with Brownian motion. In a typical DLS experiment, a beam of polarized light, usually a LASER, passes through a scattering medium. A detector measures the scattered light at a fixed angle, called scattering

angle θ [90]. Due to Brownian motion, there are fluctuations in the intensity of the scattered light, which can be measured and then interpreted by autocorrelation, using the following correlation function:

$$g_2(q,t)=\frac{1}{\langle I\rangle^2}\lim_{T\to\infty}\frac{1}{T}\int_0^T I(q,t)I(q,t+\tau)d\tau-1 \quad (1)$$

where I is the scattered light intensity, <I> is the temporal average scattered light intensity and t is the acquisition time, q is the scattering vector defined as q = (4πn/λ)sin(θ/2), being n the refraction index of the solvent, λ the light wavelength and θ the scattering angle. We can determine the field autocorrelation function g1 through the Segret relation g2 = | g1|2. For monodisperse non-interacting particles in Brownian motion, this function is a simple decreasing exponential with a relaxation rate Γ (Γ = 1 / τ, τ = decay time)[91].

This relaxation rate is obtained by curve fit, and can then be related to particle size. To do so, it is necessary to determine the coefficient diffusion of suspended particles, which is one of the processes of Brownian motion. Brownian motion is a random, microscopical movement, which results from thermal fluctuations in the fluid medium. In his seminal paper, Einstein stated that one of the processes that determines particle movement in a suspension was "a process of diffusion, which is to be looked upon as a result of the irregular movement of the particles produced by the thermal molecular movement", and he then proceeded in defining the coefficient of diffusion (D) for spherical particles as:

$$D=\frac{K_B T}{6\pi\eta r_h} \quad (2)$$

where K_B is the Boltzman's constant (minding that K_B=R/NA), T is the temperature of the medium, η is the fluid's viscosity, and r_h is the hydrodynamic radius [92], in which one is interested for particle sizing. Relaxation rate relates to coefficient diffusion through the equation:

$$\Gamma = qD^2 \quad (3)$$

So, by experimentally determining Γ, we can determine particle size in suspension by using equations (2) and (3). For monodisperse solutions, g1 has only one exponential decay, but for polydisperse solutions, g1 shows several exponential decay components, and interpretation of DLS data requires either cumulant or multi-exponential analysis [91]. Modern DLS particle sizing apparatus

are already equipped with autocorrelators, are fully automated, and able to determine particle size and polydispersity index (PDI) of nanosuspensions.

In the present work, particle size was measured using a BI-MAS DLS instrument (Brookhaven Instruments, USA), operating at scattering angle of 90°, a temperature of 25 °C, pH 7.4, with dust-cutoff set to 30. At each measurement, 6 runs of 2 min each were performed. Prior to the measurements, formulations were diluted (1:100) and filtered with a syringe filter (800 nm).

3.2.2 Zeta potential

Due to their large surface area/volume ratio, the properties of the surface of nanoparticles play an important role in their overall properties, such as particle-particle interaction and particle-cell interaction. One of this properties is surface charge, yet, it is difficult to achieve satisfactory measurements, directly or otherwise, of surface electric potential [93]. Other than that, such potential causes a binding of water molecules and ions to the nanoparticle surface, creating a layer that moves along with the nanoparticle [94, Ch. 5]. Thus, it becomes important to determine the electric potential at a certain distance of the surface, characterized by the length of this layer, at the called slipping or shear plane. The electric potential at this distance is called the electrokinetic or Zeta (ζ) potential [95] – see figure 10. ζ-potential plays an important role in the stability of colloidal systems, and shelve stability is an important factor to consider when developing a new drug delivery system [96].

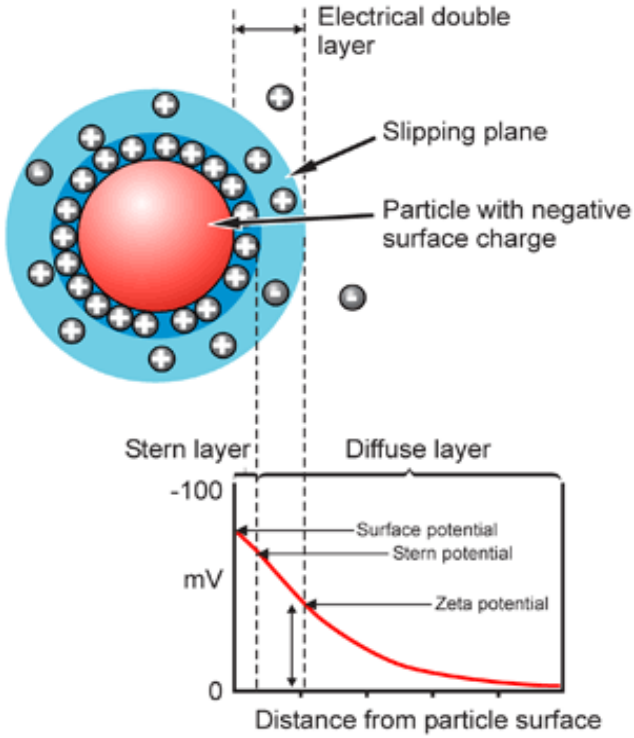

Figure 10: Illustration of variations in the electric potential from the surface of a nanoparticle.[102]

One of the most used methods to determine ζ - potential of suspended particles, and the one used in the present work, is the method of Electrophoretic Light Scattering (ELS) [93]. Since it is also a light scattering technique, it can be performed in the same apparatus as the one used for particle sizing.

In DLS, particle size is determined by measuring fluctuations in the intensity of scattered light due to Brownian motion of the suspended particles (see previous section). In ELS, two electrodes

generate an electric field, which results in a movement that overlaps Brownian motion. The frequency in scattered light thus shifts due to Doppler effect (Figure 11), and that shift (Δω) can be used to calculate particle drift velocity, through the equation:

$$\Delta \omega = q \,.\, v_d \tag{4}$$

where q is the scattering vector already discussed in the previous section. The magnitude of drift velocity is proportional to the electric field (E) by a constant, μ, which is defined as the electrophoretic mobility of the particle:

$$v_d = \mu \times E \tag{5}$$

Finally, the ζ-potential can be calculated from the electrophoretic mobility, taking electrokinetic properties of the medium into account, through mathematical models. One of these models, and the one used in this work, is the Smoluchowski equation:

$$\zeta = \frac{\eta \mu}{\varepsilon_0 \varepsilon} \tag{6}$$

where η is the viscosity of the medium, ε_0 is the permitivity of vauum, and ε is the dielectric constant of the medium [97].

ζ-potential of NLCs was measured using a BI-MAS DLS instrument (Brookhaven Instruments, USA), operating at scattering angle of 90°, a temperature of 25 °C, pH 7.4. For each measurement, 10 runs were performed.

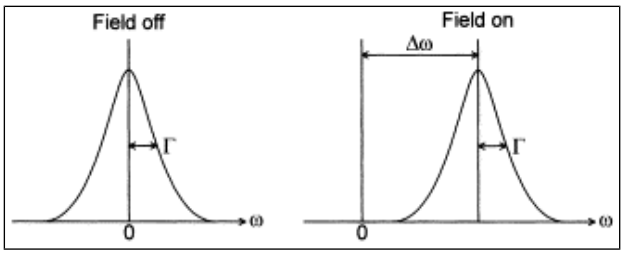

Figure 11: Frequency shift of scattered light due to movement of suspended particles when subjected to an electric field.

3.2.3 Particle morphology

Scanning Electron Microscopy (SEM) was used to observe particle morphology. In electron microscopy, a beam of charged particles (electrons) is used instead of a beam of photons (used with

optical microscopy). These particles provide beams with high energy, thus shorter wavelengths, hence allowing an observation of objects in the nanometric scale. In SEM, this beam interacts with small areas of the sample, and secondary electrons (among other particles) are scattered from it. These electrons are detected and the beam proceeds in scanning the rest of the surface. Gathered data can then be used to reconstruct the sample's morphology. The signals obtained with SEM also allow for the determination of chemical composition, crystalline structure and orientation of materials making up the sample [98].

For the present work, the SEM exam was performed using a high resolution Scanning Electron Microscope with X-Ray Microanalysis and CryoSEM experimental facilities: JEOL JSM 6301F/ Oxford INCA Energy 350/ Gatan Alto 2500. The specimen was rapidly cooled (plunging it into sub-cooled nitrogen – slush nitrogen) and transferred under vacuum to the cold stage of the preparation chamber. The specimen was fractured, sublimated ('etched') for 120 sec. At –90 °C, and coated with Au/Pd by sputtering for 45 sec. The sample was then transferred into the SEM chamber, and studied at a temperature of -150 °C.

3.2.4 Loading efficiency

The efficiency with which an active agent is incorporated into a carrier matrix can be expressed as a percentage, which is referred to as the loading efficiency (LE), and is calculated using the following expression:

$$\mathrm{LE} = \frac{T_D - U_D}{T_D} \times 100 \tag{7}$$

where T_D is total drug and U_D is unentrapped drug (drug dissolved in water medium).

The loading capacity (LC), which is the capacity of an encapsulation system to carry a drug, can be calculated by the expression:

$$LC = \frac{E_D}{E_D + \mathrm{matrix}} \times 100 \tag{8}$$

where ED is the drug entrapped in the nanosystem.

The amount of drug dissolved in water medium can be quantified by UV-Visible spectroscopy, which allows relating absorbance of radiation at a specific wavelength with the concentration of the dissolved drug.

When electromagnetic radiation interacts with matter, energy transfer may occur in many ways. In one of them, electrons in the electron cloud will absorb incident photons, as long as they have the exact same energy as it would be necessary to promote the transition from one energy level to an upper one, changing the atom or molecule's quantum mechanical states. The allowed energy levels are quantized, and are specific of the chemical species [99].

The energy of an electromagnetic wave, E, is related to it's frequency, *f*, by the expression:

$$E = h.f = \frac{c\,h}{\lambda} \tag{9}$$

where *h* is Planck's constant. Since f=c/λ, where *c* is the speed of light in vacuum and λ is the wavelength of radiation. It is therefore possible to identify elements in samples by determining for which wavelengths photons are highly absorbed from an incident beam. This set of wavelengths constitutes an absorption spectrum [100]. Absorbance of a solution is proportional to the solute's concentration, as is expressed by Beer-Lambert's law:

$$A = abc \tag{10}$$

where *c* is the solute's concentration, *b* is the length of solution the beam has to cross, and *a* is a proportionality constant. A calibration curve is usually obtained by preparing several samples, with increasing, well known concentrations, and obtaining their absorption spectrum. Prominent local maximums, indicating high absorbance at specific wavelengths, are identified. For the wavelength at a specific local maximum, and *ab* being constant, absorbance is plotted against concentration, and a linear fit should be obtained. The resulting equation is then used to determine the mass concentration of a sample, through measuring the absorbance at that particular wavelength, provided the expected concentration is inside the range used for calibration [100]. A modern spectrophotometer does an automatic and highly precise wavelength sweep, meaning it automatically changes the wavelength of the incident beam by controlling a monochromer.

The first step in the determination of incorporated drug, was to obtain a calibration curve from drug solutions with known concentrations. The determination of the concentration of the two drugs used in the present work was done with a spectrophotometer (Jasco V-660) using quartz cells. Wavelength interval ranged from 200 nm to 700 nm, with 1.0 nm intervals. The prepared concentrations of drug to determine the linear fit are presented in table 8 for RIF and in table 9 for RFB.

The second step consisted in separating the NLCs from their supernate, and then measuring the drug content of the supernate (non-loaded drug). To achieve this, formulations were diluted and

centrifuged inside centrifugal filter units (50 000 NMWL, Milipore corporation, Ireland) for 5 min at 3 500 RPM. Supernate was collected and it's drug content determined as explained before.

3.2.5 Schiff's base detection by FTIR spectroscopy

As stated before, mannose coating was done by bonding of the open chain mannose with amine terminations in the surface of the NLCs through a Schiff's base (see section 3.1.4). Fourier Transform Infrared (FTIR) spectroscopy was used to detect Shiff's base and confirm coating with mannose. FTIR spectroscopy is a technique similar to UV-Vis spectroscopy. The main differences between the two techniques reside in the wavelength of the incident beam and in the mathematical treatment of the raw data. UV-Vis spectroscopy works in the ultraviolet and visible ranges of the electromagnetic spectrum, while FTIR, as the name suggests, works in the infrared range. The difference in wavelength translates in a difference in energy, and FTIR spectroscopy is therefore able to detect energies associated with specific bonds inside molecules. The second mentioned difference is related with how the data is obtained. In UV-Vis spectroscopy, beams of very well defined wavelengths are used for each measurement. With FTIR spectroscopy, broadband beams, containing full spectrum of wavelengths, are used for each measurement. Following measurements use different spectra. The translation of raw data into absorption for each wavelength requires mathematical processing, and a Fourier transform is used. The fact that a full spectrum of wavelengths is used instead of a single wavelength beam, renders this technique faster than conventional spectroscopy.

FTIR analysis of the samples was done with a Frontier FTIR Spectrometer with universal ATR Diamond/ZnSe accessory (Perkin Elmer, USA). Samples were lyophilized as described in section 3.1.5 before FTIR analysis. Lyophilized samples were placed in ATR accessory and samples were measured from wavenumber 600 to 4 000 cm^{-1}, 50 scans per sample, with a resolution of 4 cm^{-1}.

3.2.6 Citotoxicity

Citotoxicity of the developed formulations was studied using MTT (3-[4,5-dimethylthiazol-2-yl]-2,5-diphenyltetrazolium bromide) assays with three different cell lines: Calu-3 (upper respiratory tract epithelium); A529 (lower respiratory tract epithelium) and Raw (macrophage cell lines). MTT is a water soluble salt. Cleavage of the tetrazolium ring of MTT by succinate dehydrogenase within the mitochondria results in the formation of an insoluble purple dye, which is impermeable to cell membranes. For this reason, the dye accumulates in the interior of non damaged cells. This insoluble dye can be collected and dissolved, resulting in a colored solution. Through the measurement

of the absorption of light of this solution at a specific wavelength through spectroscopy, it becomes possible to determine the amount of cells killed by a given process [101].

MTT assay was performed in the course of three days. In the first day cells were seeded to the 60 interior wells of a 96 well plate (the 36 exterior wells were filled with PBS), through the following procedure. Cells were cultivated in T25 flasks with Dulbecco's Modified Eagle Medium (DMEM) + Glutamax, complemented with PenStrep, Fungizone and Fetal Bovine Serum (all from Gibco, Life Technologies). When confluency was reached, cell medium was removed, and flasks were washed two times with phosphate buffer saline (PBS) solution, and medium was added. Cells were then detached from the flask's surface. For Raw cell lines, this was done using a scraper. To detach Calu-3 and A549 cells, a tripcine solution was added and the flasks were put to rest for 5 min at 37 ºC. Medium with suspended cells was pipetted to falcon tubes, that were then centrifuged (1 500 rpm, 5 min, 4 ºC) to separate medium with tripcine from the cell's pellet. Cells were then resuspended in DMEM. All cells were then counted using the tripanblue explosion method, with a Neubauer chamber, and cell suspensions were diluted to obtain concentrations of 25 000 cells mL^{-1}. Finally, each suspension was added to each of the 60 wells, to achieve an approximate concentration of 5 000 cells/well. Cell plates were left to rest for 24 hours, at 37 ºC.

In the second day, medium from wells was removed and cells were washed 2 times with PBS. NLC suspensions and positive and negative controls were added to the wells. Positive control was DMEM. Negative control was Triton X100 2% (m/m). Lyophilized NLCs were resuspended in DMEM. For each NLC formulation, 5 concentrations were used (1 µg mL^{-1}, 10 µg mL^{-1}, 100 µg mL^{-1}, 1 000 µg mL^{-1} 10 000 µg mL^{-1}), and for each concentration 5 wells were used. Cell plates were left to rest for 24 hours, at 37 ºC.

In the third day, MTT was added to the wells and cell plates were left to rest for 4 hours. At the end of this period, medium was removed, and Dimethyl sulfoxide (C_2H_6OS, M = 78.13 g mol^{-1}, Sigma Aldrich) was added to each well. Cell plates were protected from light and agitated for 5 minutes. Then absorptivity was measured using a multi-mode microplate reader (Synergy HT, Biotek Instruments).

This three day procedure was repeated two times for each cell line to replicate results.

4 Results and discussion

4.1 Particle size and Zeta potential

Mean hydrodynamic particle size for all formulations was found to be around 200 nm, as it is possible to see in tables 6 and 7. PDI was found to be above 0.100 in all formulations. This indicates that none of the formulations are monodisperse. As stated in section 3.2.1, prior to size and zeta measurements, formulations were filtered with a syringe filter with a porus of 800 nm. The objective of this step was to remove any excess lipid and particle agglomerates. However, it does allow particles of bigger sizes to coexist in the formulation if the method produces them. The conclusions to be taken from these results are that the method used in this work does not produce monodisperse NLC formulations without posterior filtering, but the obtained sizes are within the breathable range, and with potential to reach the pulmonary alveoli.

Table 6: Mean hydrodynamic particle size and zeta potential for unloaded formulations

	NLC	**NLC-M**
Mean size / nm	174.4 ± 2.4	197.4 ± 1.4
PDI	0.211 ± 0.012	0.120 ± 0.008
Zeta potential / mV	– 20.5 ± 0.8	48.7 ± 2.1

Results: mean ± SD ($n \geq 3$)

Results for ζ – potential listed in table 6 show that NLC have a pronounced negative charge, while NLC-M exhibit a high positive charge. These values point to a successful mannosylation of the NLCs. As described in section 3.1.4, the process of mannosylation involves adding stearyl ammine to the formulations, so that nanoparticles have amine groups at the surface. These amine groups are expected to link to mannose molecules through a Schiff's base. Amine groups are positively charged, so ζ – potential was expected to become positive. These results are also observed in table 7, with drug loaded NLCs. All mannosylated formulations exhibit positive charges, contrasting with non-mannosylated formulations. This indicates us that the presence of RIF and RFB in the formulations does not interfere with the mannosylation process.

Table 7: Mean hydrodynamic particle size and zeta potential for loaded formulations.

	NLC-RIF	NLC-M-RIF	NLC-RFB	NLC-M-RFB
Mean size / nm	210.6 ± 1.2	202.0 ± 3.5	179.1 ± 1.6	213.0 ± 1.8
PDI	0.129 ± 0.007	0.190 ± 0.008	0.114 ± 0.015	0.118 ± 0.014
Zeta potential / mV	-20.8 ± 0.9	31.9 ± 0.5	-17.9 ± 1.9	37.6 ± 1.0

Results: mean±SD (n ≥ 3)

Surface charge plays an important role in particle stability. The observed absolute values for ζ – potential are high, both for NLC and NLC-M. This indicates that the formulations are presumably stable. Stability of two formulations was monitored through time. Size and ζ – potential was measured at day 1, day 30, day 90 and day 180. Results up to day 90 are shown in figure 12 to 14. Mean size and PDI are shown for NLC (figure 1) and NLC-M (figure 2), and they do increase over time.

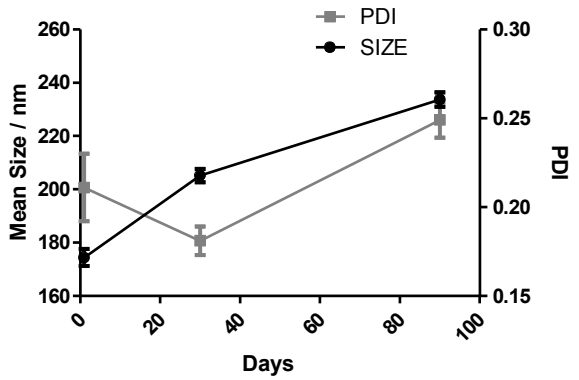

Figure 12: Mean size and PDI (± SD) of NLC.

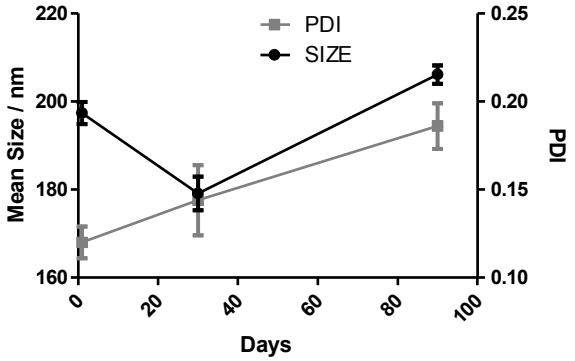

Figure 13: Mean size and PDI (± SD) of NLC-M.

Figure 14 shows a slight shift of ζ – potential torwards neutrality. However, more dramatic were the observations at day 180. These show formulations with visible particulates in suspension. DLS analysis was not possible, as the software was not able to determine a correlation function from the acquired data. This points to a shelf stability of the formulations inferior to 6 months.

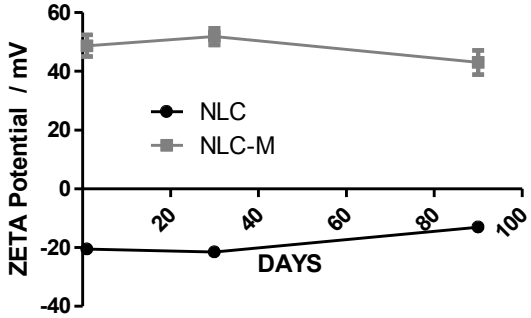

Figure 14: ζ - potential ± SD for NLC and NLC-M

4.2 Particle morphology

SEM imaging revealed spherical particles for all formulations, with sizes between 100 and 300 nm. Both these observations validate the results obtained with DLS, and the method of formulation. As we can see in figures 15A to 15B, it can be observed that both NLC and NLC-M formulations exhibit similar morphologies, indicating that the method of mannosylation does not have an effect on particle shape. However, images for NLC-M do show smaller particles than NLC. A possible explanation is that such is simply due to the polidispersity. Different regions may exhibit differences in observed sizes. To test this hypothesis, a greater number of images should be obtained, particles should be individually counted and measured, and the results should be compared with the results from DLS.

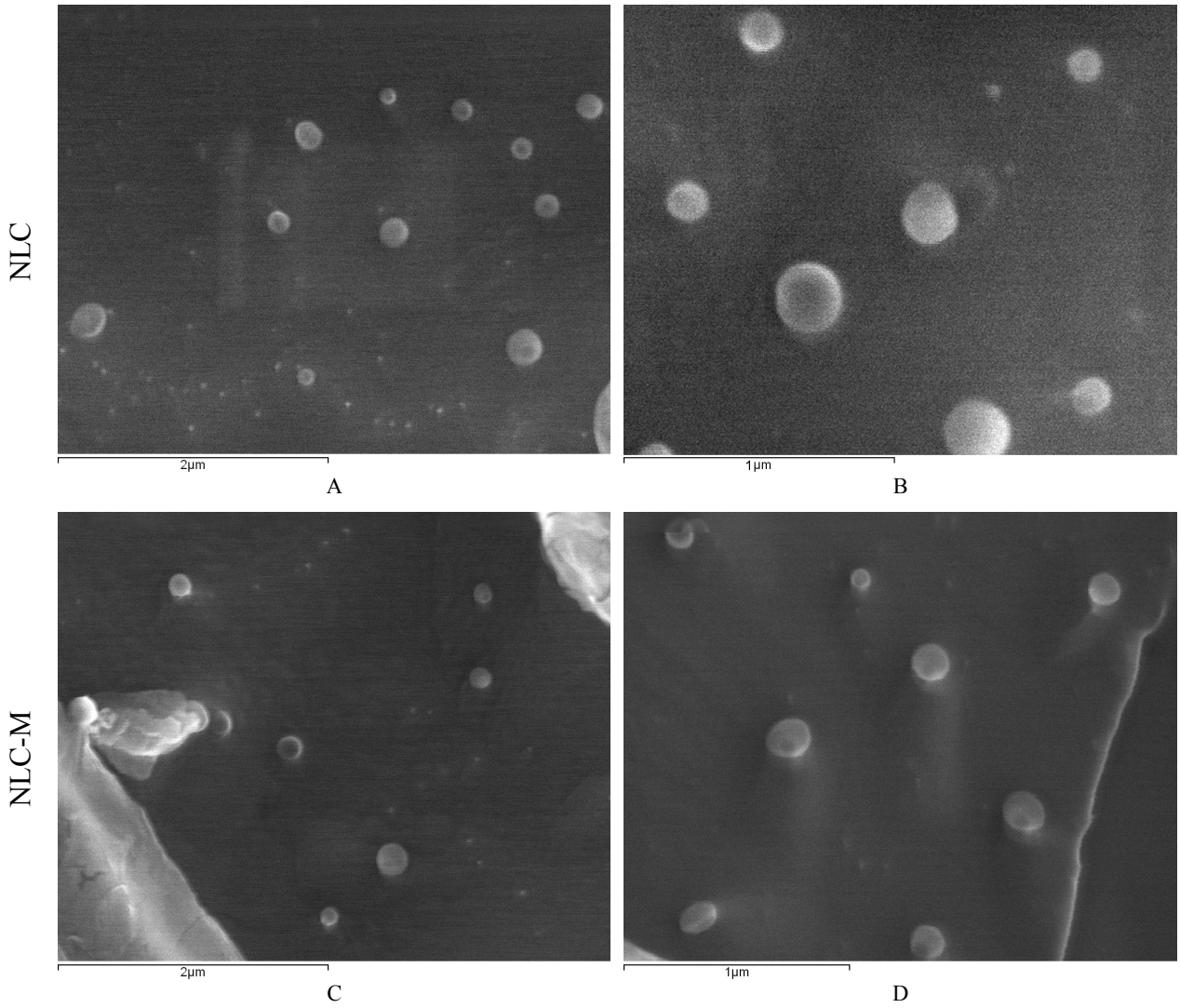

Figure 15: SEM images for NLC and NLC-M

From figures 16A to 16B, it can observed that loaded NLCs (NLC-RIF and NLC-RFB) also exhibit spherical shapes, which indicates that the method of drug loading is also not resulting in morphological changes. The variability of sizes seems to be higher in drug loaded NLCs (this is more visible in NLC-RIF images) than with empty NLCs, but this was not observed in PDI measured with DLS. Again, the region of observation plays an important role in the perception of the characteristics of each sample, reinforcing the complementary nature of the different methods used to evaluate particles size and PDI.

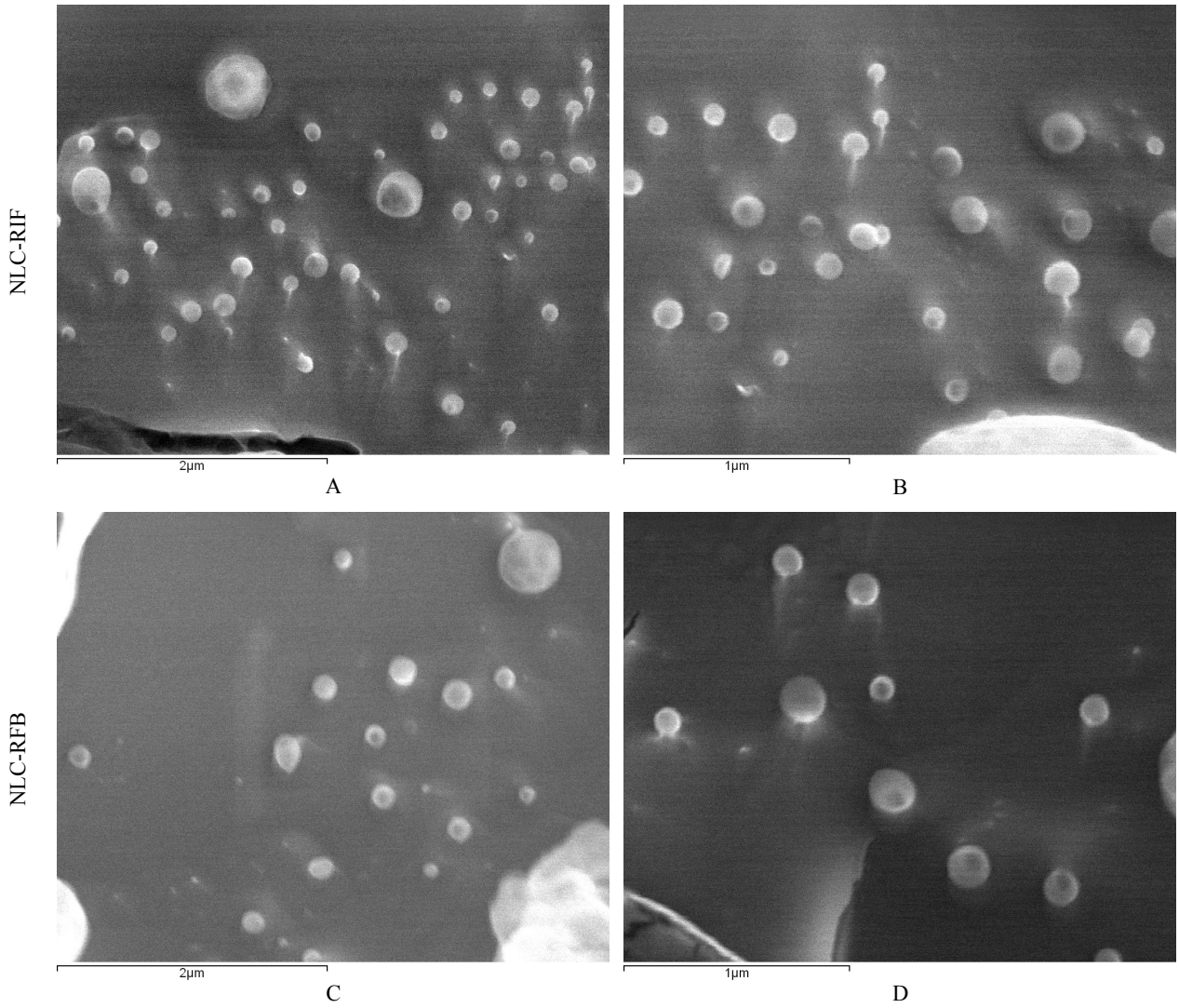

Figure 16: SEM images for NLC-RIF and NLC-RFB

4.3 Loading efficiency

Figures 17 and 18 show spectrograms for the absorbance obtained by NLC-RIF and NLC-RFB, respectively. For RIF, spectrum showed three interesting local maximums at 255, 334 and 473 nm. Linear fit of the plot of concentration versus absorbance was obtained, and wavelength for 334 nm showed greater R^2 value. For RFB, spectrogram showed interesting local maximums at 208, 279 and 319 nm. Linear fit of the plot of concentration versus absorbance resulted in wavelength 208 nm showing greater R^2 value.

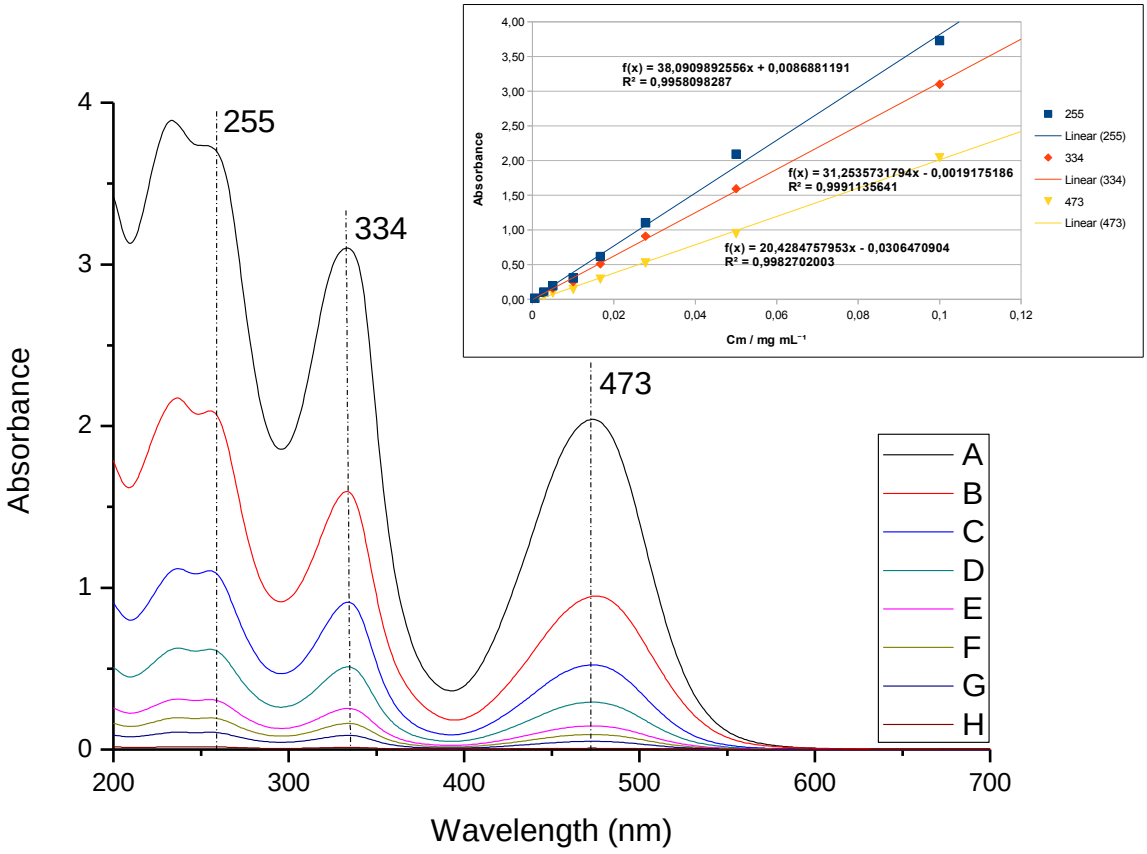

Figure 17: Calibration spectrum and linear fit for RIF.

Table 8: Concentrations of RIF solutions used in dosing calibration.

	Solutions							
	A	**B**	**C**	**D**	**E**	**F**	**G**	**H**
Cm / mg mL^{-1}	0.1000	0.0500	0.0278	0.0167	0.0100	0.0050	0.0028	0.0006

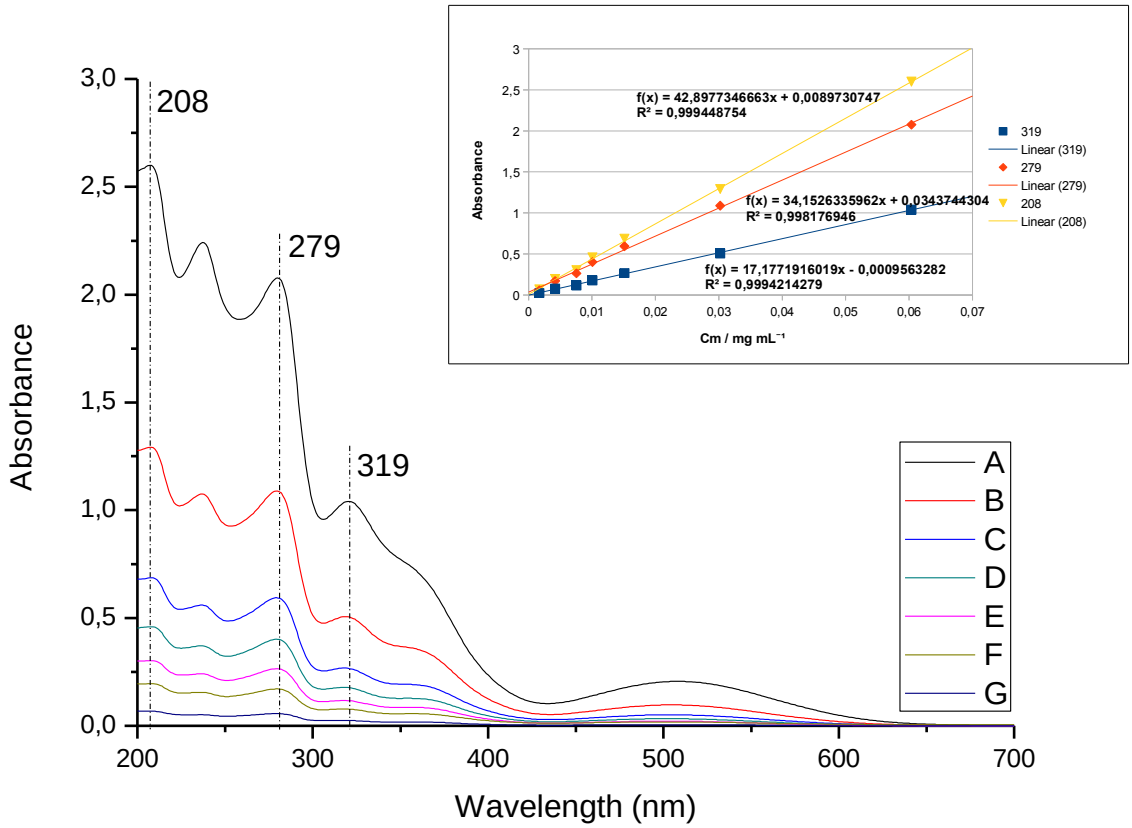

Figure 18: Calibration spectrum and linear fit for RFB.

Table 9: Concentrations of RFB solutions used in dosing calibration.

	Solutions						
	A	**B**	**C**	**D**	**E**	**F**	**G**
Cm / mg mL^{-1}	0.0604	0.0302	0.0151	0.0101	0.0075	0.0042	0.0017

Spectrophotometric results for drug presence in the supernate of formulations showed low absorbances, and calculations yielded high loading efficiencies for all formulations (table 10). Mannosylated NLCs did not exhibit reduced loading efficiencies, so the technique may be used without it reducing the capacity of the nanosystem to incorporate these two drugs.

Table 10: Loading efficiency for non coated and coated formulations.

	NLC-RIF	**NLC-M-RIF**	**NLC-RFB**	**NLC-M-RFB**
LE / %	84.1 ± 5.0	82.7 ± 3.3	82.4 ± 5.6	89.4 ± 3.4

Drug to lipid ratio: aprox. 1:70. Results: Mean ± SD (n=3)

4.4 Schiff's base detection

Results obtained for ζ – potential already indicated that mannose coating was probably achieved with success. This was confirmed by the obtained FTIR peaks. Figure 19 shows a broad peak at 1566 cm^{-1} in NLC-M, indicating an N=C connection. This confirms the formation of Schiff's base (– N=CH –) in NLC-M, and its absence in NLC [87].

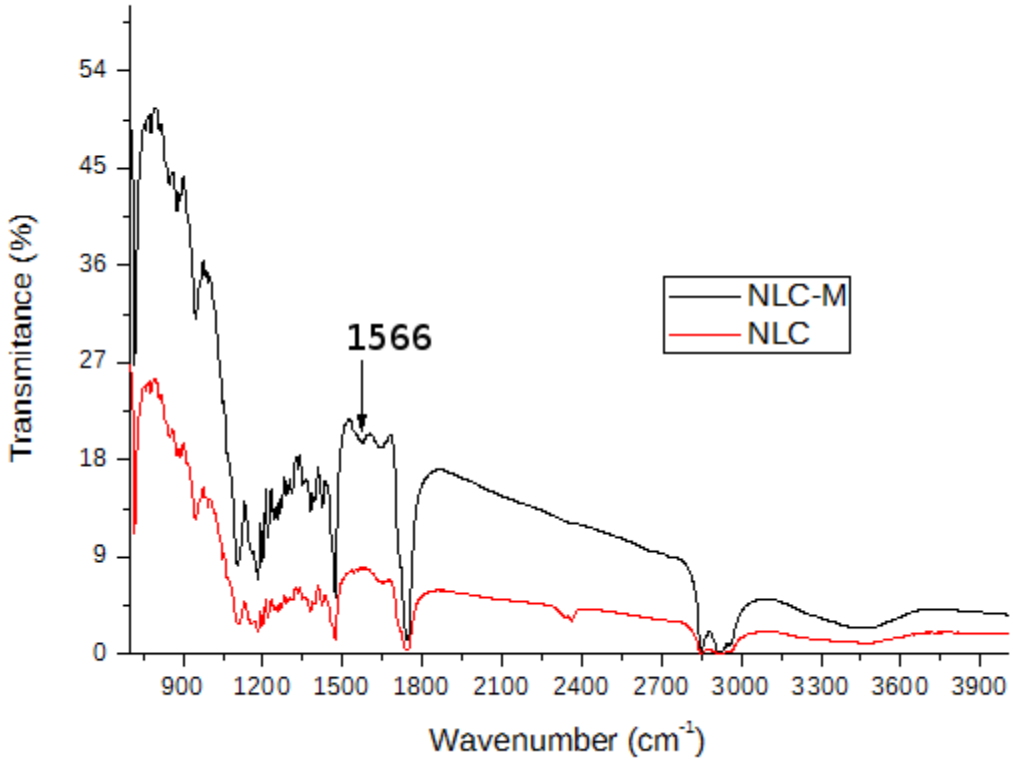

Figure 19: FTIR spectra of NLC and NLC-M.

4.5 Citotoxicity

Half maximum inhibitory concentration (IC50) was determined for all cell lines, from the viability results of each for NLC, NLC-M, NLC-M-RIF and NLC-M-RFB. Table 11 summarizes these results. Figures 20, 21 and 22 show the results for RAW, Calu-3 and A549 cell lines, respectively.

IC50 for all formulations and cell lines was above 100 µg mL^{-1} (Log_{10}(IC50) > 2), but bellow 1 000 µg mL^{-1}. NLC-M constitutes, however, a notorious exception to this observation, exhibiting, for all cell lines, an IC50 bellow 100 µg mL^{-1} (Log_{10}(IC50) < 2). Drug loaded formulations, although mannosylated, did not show this behaviour. Indeed, the loaded drugs seem to lower the toxicity of the cell lines in the presence of mannose, rendering the IC50 to values similar to the obtained for NLC in the absence of mannose.

Table 11: IC50 results for RAW, CALU-3 and A549 cell lines.

	NLC	NLC-M	NLC-M-RIF	NLC-M-RFB
RAW	2.120 ± 0.267	1.276 ± 0.654	2.215 ± 0.231	2.036 ± 0.844
CALU-3	2.706 ± 0.178	1.482 ± 0.772	2.840 ± 0.265	2.378 ± 0.253
A549	2.259 ± 0.095	1.272 ± 0.452	2.552 ± 0.592	2.269 ± 0.592

Results: Log_{10}(IC50) ± SE

Figure 20 shows cell viability (A) and curve fit (B) RAW cell line. IC50 for NLC, NLC-M, NLC-M-RIF, and NLC-M-RFB was 131.9 µg mL^{-1}, 18.88 µg mL^{-1}, 164.2 µg mL^{-1}, and 108.7 µg mL^{-1}, respectively. Although only NLC-M exhibit an IC50 bellow 100 µg mL^{-1}, individual results for RAW cell line show that for NLC formulation, a concentration of 100 resulted in a cell viability only little above 50%. NLC-M-RFB showed a lower viability than the other formulations with concentrations of 1 and 10 µg mL^{-1}.

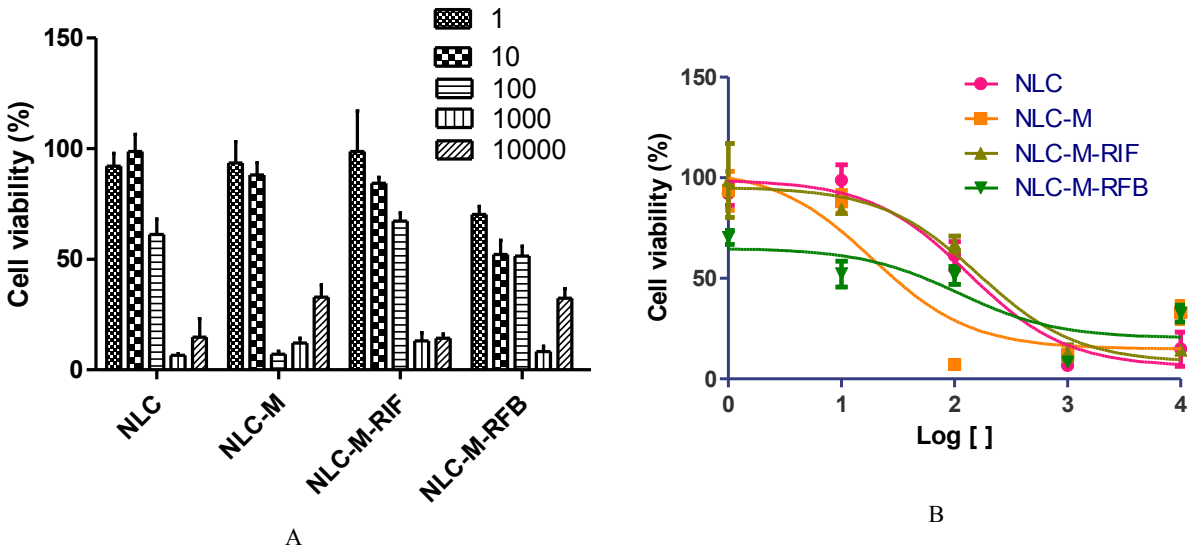

Figure 20: MTT results for Raw cell line (Mean ± SD).

Figure 21 shows cell viability (A) and curve fit (B) for CALU-3 cell line. IC50 for NLC, NLC-M, NLC-M-RIF, and NLC-M-RFB was 508.5 µg mL^{-1}, 30.3 µg mL^{-1}, 691.3 µg mL^{-1}, and 238.9 µg mL^{-1}, respectively. CALU-3 cell line showed higher cell viability than both RAW and A549 cell lines, for all formulations, although it also exhibits a drop in IC50 for the NLC-M formulation.

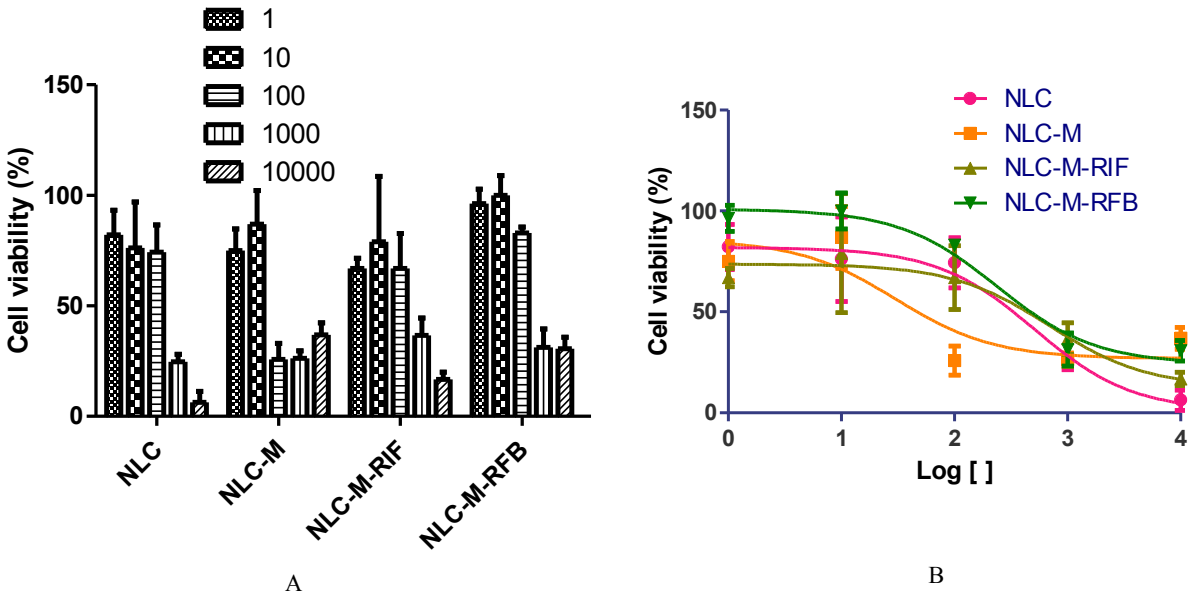

Figure 21: MTT results for CALU-3 cell line (Mean ± SD).

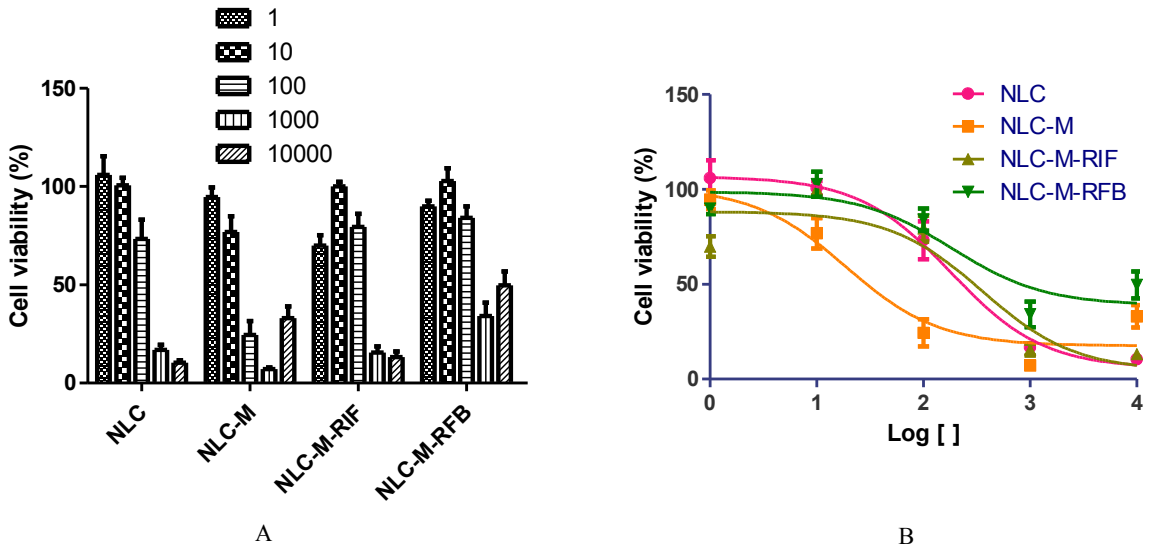

Figure 22: MTT results for A549 cell line (Mean ± SD).

Figure 22 shows cell viability (A) and curve fit (B) for A549 cell line. IC50 for NLC, NLC-M, NLC-M-RIF, and NLC-M-RFB was 181.5 μg mL^{-1}, 18.7 μg mL^{-1}, 356.7 μg mL^{-1}, and 185.7 μg mL^{-1}, respectively.

Drug loaded NLCs have a drug content of around 1% (w/w) (see section 4.3). Considering IC50 values for the studied cell lines, it therefore becomes possible, with these formulations, to achieve maximum drug concentrations, at the site of delivery, between 1.08 μg mL^{-1} and 6.91 μg mL^{-1}.

5 Conclusions and future prospects

With the presented method, it was possible to develop formulations consisting of NLCs coated with mannose and loaded with RIF and RFB. The size of the produced particles was determined by DLS and found to be around 200 nm, which should be adequate for lung deposition, based on data found in the scientific literature. This validates the proposed route of administration, which was the pulmonary route. With this passive targeting strategy, NLCs of this size are expected to reach the pulmonary alveoli. A breathable formulation presents many advantages in the case of TB, since the MTb exists primarily inside the AMs, in the pulmonary alveoli. A strategy that succeeds in deliver anti-TB drugs directly to the alveoli may increase treatment efficacy, and, on the other hand, it may suite the needs of a strategy to overcome patient non-compliance. ζ – potential was considerably high for all formulations, which suggested a fairly good shelf life stability. Further stability studies showed that diluted formulations had a shelf life of at least 3 months, but probably no longer than 6 months. Lyophilization of the formulation may be used to solve this issue.

Mannose surface modification was done to take advantage of sugar receptors in AMs and improve cellular uptake, an active targeting strategy. The difference in the ζ – potential between the non mannosylated and the mannosylated NLCs constituted the first evidence that the mannosylation process was successful. This was later confirmed by FTIR spectrum analysis, which allowed for the detection of a Schiff's base.

Morphology of the NLCs was studied by SEM imaging. Results showed spherical particles, with sizes consistent with DLS analysis. The variability in the observed sizes is explained by the PDI of the formulations. To obtain formulations with lower PDI values, such that they could be considered monodisperse, filtration could be done with porous of lower diameters, such as 450 nm or even 200 nm. In industry, other methods to produce NLCs could be used, and some of them, like high pressure homogenization, will naturally produce monodisperse populations of particles.

Another positive and promising achievement of this work, were the results regarding drug loading. To optimize the formulation and improve drug loading, several solid lipids were tested, and

Precirol ATO 5 was chosen for the final formulation. This resulted in LE that ranged from 82.4 ± 5.7 % to 87.5 ± 4.6 %, for a drug to lipid ratio of approximately 1:70.

Cytotoxicity of the NLCs was studied by MTT assay, using RAW, CALU-3 and A549 cell lines. Results showed that it was possible to reach concentrations above 100 and below 1 000 μg mL^{-1} before IC50 was reached, for drug loaded formulations. Other toxicity studies, such as the lactate dehydrogenase assay, could be used in the future to complement these results. Other *in vitro* studies may shed a light on the real possibilities of these nanocarriers. Cellular uptake studies should be performed to access if the use of NLCs does enhance the uptake of drugs, and if mannose coating indeed improves these values.

After all *in vitro* studies are duly performed, *in vivo* studies should be considered. These studies should be planned to answer some pertinent questions. Will the delivery strategy allow for the drug to reach the circulatory and lymphatic systems, hence be used to fight extra-pulmonary TB? Will the particles achieve a successful deposition in the pulmonary alveoli? If so, will they truly enhance cellular uptake of RIF and RFB, reducing side effects and enhancing bioavailability?

These further studies may present this strategy as an important tool to fight TB, but it may find difficulties which would render it impossible to apply. So far, and despite all the studies considering the possibility, no breathable formulation for the treatment of TB is available in the market. However, from these facts it does not follow that the pursuit of an NLC formulation to fight TB should be dropped. On the contrary, these initial results are very promising, and so they should encourage us to go farther.

References

[1] "Global Tuberculosis Report," *World Health Organization*, 2012. [Online]. Available: http://www.who.int/tb/publications/global_report/en/. [Accessed: 31-Jul-2013].

[2] S. Sarkar and M. R. Suresh, "An Overview of Tuberculosis Chemotherapy - A Literature Review," *J. Pharm. Pharm. Sci.*, vol. 14, no. 2, pp. 148–161, 2011.

[3] L. Willis, D. Hayes, and H. Mansour, "Therapeutic Liposomal Dry Powder Inhalation Aerosols for Targeted Lung Delivery," *Lung*, vol. 190, no. 3, pp. 251–262, 2012.

[4] A. Aderem and D. M. Underhill, "Mechanisms of phagocytosis in macrophages," *Annu. Rev. Immunol.*, vol. 17, pp. 593–623, 1999.

[5] J. A. Armstrong and P. D. Hart, "Response of Cultured Macrophages to Mycobacterium Tuberculosis, with Observations on Fusion of Lysosomes with Phagosomes," *J. Exp. Med.*, vol. 134, no. 3, pp. 713–740, Sep. 1971.

[6] N. Krishnan, B. D. Robertson, and G. Thwaites, "The mechanisms and consequences of the extra-pulmonary dissemination of Mycobacterium tuberculosis," *Tuberculosis (Edinb)*, vol. 90, no. 6, pp. 361–366, Nov. 2010.

[7] J. L. Flynn and J. Chan, "Immunology of Tuberculosis," *Annu. Rev. Immunol.*, vol. 19, no. 1, pp. 93–129, 2001.

[8] N. E. Dunlap, J. Bass, P. Fujiwara, P. Hopewell, C. R. Horsburgh, M. Salfinger, and P. M. Simone, "Diagnostic standards and classification of tuberculosis in adults and children," *Am. J. Respir. Crit. Care Med.*, vol. 161, no. 4, pp. 1376–1395, Apr. 2000.

[9] J. H. Grosset, T. G. Singer, and W. R. Bishai, "New drugs for the treatment of tuberculosis: hope and reality," *Int. J. Tuberc. Lung Dis.*, vol. 16, no. 8, pp. 1005–1014, 2012.

[10] J. G. Douglas and M. J. McLeod, "Pharmacokinetic factors in the modern drug treatment of tuberculosis," *Clin Pharmacokinet*, vol. 37, no. 2, pp. 127–146, 1999.

[11] M. A. Espinal, S. J. Kim, P. G. Suarez, K. M. Kam, A. G. Khomenko, G. B. Migliori, J. Baez, A. Kochi, C. Dye, and M. C. Raviglione, "Standard short-course chemotherapy for drug-resistant tuberculosis - Treatment outcomes in 6 countries," *JAMA-J. Am. Med. Assoc.*, vol. 283, no. 19, pp. 2537–2545, May 2000.

[12] R. Shi, N. Itagaki, and I. Sugawara, "Overview of anti-tuberculosis (TB) drugs and their resistance mechanisms," *Mini Rev Med Chem*, vol. 7, no. 11, pp. 1177–1185, Nov. 2007.

[13] "Press Announcements - FDA approves first drug to treat multi-drug resistant tuberculosis." [Online]. Available: http://www.fda.gov/NewsEvents/Newsroom/PressAnnouncements/ucm333695.htm. [Accessed: 14-Jul-2013].

[14] A. Misra, A. J. Hickey, C. Rossi, G. Borchard, H. Terada, K. Makino, P. B. Fourie, and P. Colombo, "Inhaled drug therapy for treatment of tuberculosis," *Tuberculosis (Edinb)*, vol. 91, no. 1, pp. 71–81, Jan. 2011.

[15] T. Sethi and A. Agrawal, "Structure and function of the tuberculous lung: Considerations for inhaled therapies," *Tuberculosis (Edinb)*, vol. 91, no. 1, pp. 67–70, Jan. 2011.

[16] D. A. Hokey and A. Misra, "Aerosol vaccines for tuberculosis: A fine line between protection and pathology," *Tuberculosis*, vol. 91, no. 1, pp. 82–85, Jan. 2011.

[17] A. Amani, M. A. Amini, H. S. M. Ali, and P. York, "Alternatives to Conventional Suspensions for Pulmonary Drug Delivery by Nebulisers: A Review," *J. Pharm. Sci.*, vol. 100, no. 11, pp. 4563–4570, Nov. 2011.

[18] P. Muttil, C. Wang, and A. Hickey, "Inhaled Drug Delivery for Tuberculosis Therapy," *Pharm. Res.*, vol. 26, no. 11, pp. 2401–2416, 2009.

[19] J. C. Sung, B. L. Pulliam, and D. A. Edwards, "Nanoparticles for drug delivery to the lungs," *Trends in Biotechnology*, vol. 25, no. 12, pp. 563–570, Dec. 2007.

[20] S. Gill, R. Löbenberg, T. Ku, S. Azarmi, W. Roa, and E. J. Prenner, "Nanoparticles: Characteristics, Mechanisms of Action, and Toxicity in Pulmonary Drug DeliveryA Review," *J. Biomed. Nanotechnol.*, vol. 3, no. 2, pp. 107–119, 2007.

[21] A. H. L. Chow, H. H. Y. Tong, P. Chattopadhyay, and B. Y. Shekunov, "Particle engineering for pulmonary drug delivery," *Pharm. Res.*, vol. 24, no. 3, pp. 411–437, Mar. 2007.

[22] C. Bosquillon, C. Lombry, V. Preat, and R. Vanbever, "Influence of formulation excipients and physical characteristics of inhalation dry powders on their aerosolization performance," *J. Control. Release*, vol. 70, no.

3, pp. 329–339, Feb. 2001.

[23] A. B. Yadav, A. K. Singh, R. K. Verma, M. Mohan, A. K. Agrawal, and A. Misra, "The devil's advocacy: When and why inhaled therapies for tuberculosis may not work," *Tuberculosis (Edinb)*, vol. 91, no. 1, pp. 65–66, Jan. 2011.

[24] N. Nimje, A. Agarwal, G. K. Saraogi, N. Lariya, G. Rai, H. Agrawal, and G. P. Agrawal, "Mannosylated nanoparticulate carriers of rifabutin for alveolar targeting," *J. Drug Target.*, vol. 17, no. 10, pp. 777–787, 2009.

[25] S. K. Jain, Y. Gupta, L. Ramalingam, A. Jain, A. Jain, P. Khare, and D. Bhargava, "Lactose-Conjugated PLGA Nanoparticles for Enhanced Delivery of Rifampicin to the Lung for Effective Treatment of Pulmonary Tuberculosis," *PDA J. Pharm. Sci. Technol.*, vol. 64, no. 3, pp. 278–287, Jun. 2010.

[26] M. Pinheiro, M. Lúcio, J. L. Lima, and S. Reis, "Liposomes as drug delivery systems for the treatment of TB," *Nanomedicine*, vol. 6, no. 8, pp. 1413–1428, Oct. 2011.

[27] S. M. Moghimi, A. C. Hunter, and J. C. Murray, "Nanomedicine: current status and future prospects," *FASEB J.*, vol. 19, no. 3, pp. 311–330, Mar. 2005.

[28] L. Gao, G. Liu, J. Ma, X. Wang, L. Zhou, and X. Li, "Drug nanocrystals: In vivo performances," *J. Control. Release*, vol. 160, no. 3, pp. 418–430, Jun. 2012.

[29] R. Shegokar, L. Al Shaal, and K. Mitri, "Present status of nanoparticle research for treatment of tuberculosis.," *J. Pharm. Pharm. Sci.*, vol. 14, no. 1, 2011.

[30] L. Plapied, N. Duhem, A. des Rieux, and V. Préat, "Fate of polymeric nanocarriers for oral drug delivery," *Curr. Opin. Colloid Interface Sci.*, vol. 16, no. 3, pp. 228–237, Jun. 2011.

[31] M. Beck-Broichsitter, O. M. Merkel, and T. Kissel, "Controlled pulmonary drug and gene delivery using polymeric nano-carriers," *J. Control. Release*, vol. 161, no. 2, pp. 214–224, Jul. 2012.

[32] E. Rytting, J. Nguyen, X. Wang, and T. Kissel, "Biodegradable polymeric nanocarriers for pulmonary drug delivery," *Expert Opin. Drug Deliv.*, vol. 5, no. 6, pp. 629–639, Jun. 2008.

[33] J. Nguyen, T. W. J. Steele, O. Merkel, R. Reul, and T. Kissel, "Fast degrading polyesters as siRNA nano-carriers for pulmonary gene therapy," *J. Control. Release*, vol. 132, no. 3, pp. 243–251, Dec. 2008.

[34] K. Tahara, H. Yamamoto, H. Takeuchi, and Y. Kawashima, "Development of gene delivery system using PLGA nanospheres," *Yakugaku Zasshi-J. Pharm. Soc. Jpn.*, vol. 127, no. 10, pp. 1541–1548, 2007.

[35] D. K. Jensen, L. B. Jensen, S. Koocheki, L. Bengtson, D. Cun, H. M. Nielsen, and C. Foged, "Design of an inhalable dry powder formulation of DOTAP-modified PLGA nanoparticles loaded with siRNA," *J. Control. Release*, vol. 157, no. 1, pp. 141–148, Jan. 2012.

[36] S. Al-Qadi, A. Grenha, D. Carrion-Recio, B. Seijo, and C. Remunan-Lopez, "Microencapsulated chitosan nanoparticles for pulmonary protein delivery: In vivo evaluation of insulin-loaded formulations," *J. Control. Release*, vol. 157, no. 3, pp. 383–390, Feb. 2012.

[37] Y. Kawashima, H. Yamamoto, H. Takeuchi, S. Fujioka, and T. Hino, "Pulmonary delivery of insulin with nebulized DL-lactide/glycolide copolymer (PLGA) nanospheres to prolong hypoglycemic effect," *J. Control. Release*, vol. 62, no. 1–2, pp. 279–287, Nov. 1999.

[38] D. Jain and R. Banerjee, "Comparison of ciprofloxacin hydrochloride-loaded protein, lipid, and chitosan nanoparticles for drug delivery," *J. Biomed. Mater. Res. Part B*, vol. 86B, no. 1, pp. 105–112, Jul. 2008.

[39] A. Zahoor, S. Sharma, and G. K. Khuller, "Inhalable alginate nanoparticles as antitubercular drug carriers against experimental tuberculosis," *Int. J. Antimicrob. Agents*, vol. 26, no. 4, pp. 298–303, Oct. 2005.

[40] G. K. Saraogi, B. Sharma, B. Joshi, P. Gupta, U. D. Gupta, N. K. Jain, and G. P. Agrawal, "Mannosylated gelatin nanoparticles bearing isoniazid for effective management of tuberculosis," *J. Drug Target.*, vol. 19, no. 3, pp. 219–227, Apr. 2011.

[41] J. M. A. Abdulla, Y. T.-F. Tan, and Y. Darwis, "Rehydrated Lyophilized Rifampicin-Loaded mPEG-DSPE Formulations for Nebulization," *AAPS PharmSciTech*, vol. 11, no. 2, pp. 663–671, Jun. 2010.

[42] A. Grenha, B. Seijo, and C. Remunan-Lopez, "Microencapsulated chitosan nanoparticles for lung protein delivery," *Eur. J. Pharm. Sci.*, vol. 25, no. 4–5, pp. 427–437, Aug. 2005.

[43] K. Sharma, S. Somavarapu, A. Colombani, N. Govind, and K. M. G. Taylor, "Cross linked chitosan nanoparticle formulations for delivery from pressurized metered dose inhalers," *Eur. J. Pharm. Biopharm.*, vol. 81, no. 1, pp. 74–81, May 2012.

[44] P. S. Pourshahab, K. Gilani, E. Moazeni, H. Eslahi, M. R. Fazeli, and H. Jamalifar, "Preparation and characterization of spray dried inhalable powders containing chitosan nanoparticles for pulmonary delivery of isoniazid," *J. Microencapsul.*, vol. 28, no. 7, pp. 605–613, 2011.

[45] J. C. Sung, D. J. Padilla, L. Garcia-Contreras, J. L. VerBerkmoes, D. Durbin, C. A. Peloquin, K. J. Elbert, A. J. Hickey, and D. A. Edwards, "Formulation and Pharmacokinetics of Self-Assembled Rifampicin Nanoparticle Systems for Pulmonary Delivery," *Pharm. Res.*, vol. 26, no. 8, pp. 1847–1855, Aug. 2009.

[46] R. Pandey, A. Sharma, A. Zahoor, S. Sharma, G. K. Khuller, and B. Prasad, "Poly (DL-lactide-co-glycolide) nanoparticle-based inhalable sustained drug delivery system for experimental tuberculosis," *J. Antimicrob. Chemother.*, vol. 52, no. 6, pp. 981–986, Dec. 2003.

[47] A. Sharma, S. Sharma, and G. K. Khuller, "Lectin-functionalized poly (lactide-co-glycolide) nanoparticles as oral/aerosolized antitubercular drug carriers for treatment of tuberculosis," *J. Antimicrob. Chemother.*, vol. 54, no. 4, pp. 761–766, Oct. 2004.

[48] W. S. Cheow and K. Hadinoto, "Enhancing encapsulation efficiency of highly water-soluble antibiotic in poly(lactic-co-glycolic acid) nanoparticles: Modifications of standard nanoparticle preparation methods," *Colloid Surf. A-Physicochem. Eng. Asp.*, vol. 370, no. 1–3, pp. 79–86, Nov. 2010.

[49] W. S. Cheow and K. Hadinoto, "Factors affecting drug encapsulation and stability of lipid-polymer hybrid nanoparticles," *Colloid Surf. B-Biointerfaces*, vol. 85, no. 2, pp. 214–220, Jul. 2011.

[50] M. Bivas-Benita, K. E. van Meijgaarden, K. Franken, H. E. Junginger, G. Borchard, T. H. M. Ottenhoff, and A. Geluk, "Pulmonary delivery of chitosan-DNA nanoparticles enhances the immunogenicity of a DNA vaccine encoding HLA-A*0201-restricted T-cell epitopes of Mycobacterium tuberculosis," *Vaccine*, vol. 22, no. 13–14, pp. 1609–1615, Apr. 2004.

[51] S. Chono, K. Kaneko, E. Yamamoto, K. Togami, and K. Morimoto, "Effect of surface-mannose modification on aerosolized liposomal delivery to alveolar macrophages," *Drug Dev. Ind. Pharm.*, vol. 36, no. 1, pp. 102–107, Jan. 2010.

[52] W. Wijagkanalan, S. Kawakami, M. Takenaga, R. Igarashi, F. Yamashita, and M. Hashida, "Efficient targeting to alveolar macrophages by intratracheal administration of mannosylated liposomes in rats," *J. Control. Release*, vol. 125, no. 2, pp. 121–130, Jan. 2008.

[53] S. Chono, T. Tanino, T. Seki, and K. Morimoto, "Uptake characteristics of liposomes by rat alveolar macrophages: influence of particle size and surface mannose modification," *J. Pharm. Pharmacol.*, vol. 59, no. 1, pp. 75–80, Jan. 2007.

[54] F. Kong, F. Zhou, L. Ge, X. Liu, and Y. Wang, "Mannosylated liposomes for targeted gene delivery," *Int. J. Nanomedicine*, vol. 7, pp. 1079–1089, 2012.

[55] O. R. Justo and A. M. Moraes, "Incorporation of antibiotics in liposomes designed for tuberculosis therapy by inhalation," *Drug Deliv.*, vol. 10, no. 3, pp. 201–207, Sep. 2003.

[56] S. Anabousi, E. Kleemann, U. Bakowsky, T. Kissel, T. Schmehl, T. Gessler, W. Seeger, C.-M. Lehr, and C. Ehrhardt, "Effect of PEGylation on the stability of liposomes during nebulisation and in lung surfactant," *J. Nanosci. Nanotechnol.*, vol. 6, no. 9–10, pp. 3010–3016, Oct. 2006.

[57] S. Chattopadhyay, S. Ehrman, J. Bellare, and C. Venkataraman, "Morphology and bilayer integrity of small liposomes during aerosol generation by air-jet nebulisation," *J. Nanopart. Res.*, vol. 14, no. 4, pp. 1–15, 2012.

[58] P. K. Gaur, S. Mishra, V. B. Gupta, M. S. Rathod, S. Purohit, and B. A. Savla, "Targeted drug delivery of Rifampicin to the lungs: formulation, characterization, and stability studies of preformed aerosolized liposome and in situ formed aerosolized liposome," *Drug Dev. Ind. Pharm.*, vol. 36, no. 6, pp. 638–646, Jun. 2010.

[59] W. H. Finlay and J. P. Wong, "Regional lung deposition of nebulized liposome-encapsulated ciprofloxacin," *Int. J. Pharm.*, vol. 167, no. 1–2, pp. 121–127, Jun. 1998.

[60] T. R. Desai, J. P. Wong, R. E. W. Hancock, and W. H. Finlay, "A novel approach to the pulmonary delivery of liposomes in dry powder form to eliminate the deleterious effects of milling," *J. Pharm. Sci.*, vol. 91, no. 2, pp. 482–491, Feb. 2002.

[61] T. R. Desai, R. E. W. Hancock, and W. H. Finlay, "A facile method of delivery of liposomes by nebulization," *J. Control. Release*, vol. 84, no. 1–2, pp. 69–78, Nov. 2002.

[62] R. Bhavane, E. Karathanasis, and A. V. Annapragada, "Triggered release of ciprofloxacin from nanostructured agglomerated vesicles," *Int. J. Nanomedicine*, vol. 2, no. 3, pp. 407–418, 2007.

[63] G. Chimote and R. Banerjee, "In Vitro Evaluation of Inhalable Isoniazid-Loaded Surfactant Liposomes as an Adjunct Therapy in Pulmonary Tuberculosis," *J. Biomed. Mater. Res. Part B*, vol. 94B, no. 1, pp. 1–10, Jul. 2010.

[64] S. . Vyas, M. . Kannan, S. Jain, V. Mishra, and P. Singh, "Design of liposomal aerosols for improved delivery of rifampicin to alveolar macrophages," *Int. J. Pharm.*, vol. 269, no. 1, pp. 37–49, Jan. 2004.

[65] P. Deol and G. K. Khuller, "Lung specific stealth liposomes: stability, biodistribution and toxicity of liposomal antitubercular drugs in mice," *Biochim. Biophys. Acta*, vol. 1334, no. 2–3, pp. 161–172, Mar. 1997.

[66] A. Agarwal, H. Kandpal, H. P. Gupta, N. B. Singh, and C. M. Gupta, "Tuftsin-bearing liposomes as rifampin vehicles in treatment of tuberculosis in mice.," *Antimicrob. Agents Chemother.*, vol. 38, no. 3, pp. 588–593, Mar. 1994.